UNIVERSIDAD DE VALLADOLID

ESCUELA DE INGENIERIAS INDUSTRIALES

Máster en Ingeniería Química

Development of a SAFT-γ Mie group-contribution approach to modelling working fluids and its application in the computer-aided molecular and process design of ORCs

Autor:

Santiuste Martínez, Jaime

Responsable de Intercambio en la UVa

Mato Chaín, Rafael

Universidad de destino

Imperial College of Science, Technology and Medicine of London

Valladolid, Julio 2020.

TÍTULO:	Development of a SAFT-γ Mie group-contribution approach to modelling working fluids and its application in the computer-aided molecular and process design of ORCs
ALUMNO:	Santiuste Martínez, Jaime
FECHA:	Julio 2020
CENTRO:	Chemical Engineering Department, Molecular Systems Engineering (MSE)
UNIVERSIDAD:	Imperial College of Science, Technology and Medicine of London
TUTOR:	Haslam, Andrew J.

Resumen

Los ciclos de Rankine orgánicos (Organic Rankine Cycles, ORCs) se presentan como una buena alternativa para recuperar el calor residual. De entre los fluidos de trabajo posibles, los hidrofluorocarbonos (HFCs) destacan por su potencial para aumentar el rendimiento de estos ciclos.

Dentro del método SAFT-γ Mie, se han desarrollado los grupos funcionales pertenecientes a los HFCs, obteniendo una estimación de la presión de vapor y de la densidad de líquido saturado con una desviación media absoluta, respecto a los datos experimentales, de 3,17% y 1,77%, respectivamente.

Por último, una vez desarrollado el modelo termodinámico con la ecuación SAFT-γ Mie y analizadas las propiedades de transporte, se propone un marco para el diseño molecular y de proceso asistido por ordenador (Computer-Aided Molecular and Process Design, CAMPD), con el objetivo de maximizar la potencia obtenida con el ciclo, modificando para ello tanto el fluido de trabajo como las condiciones de operación.

Palabras clave

Abstract

Organic Rankine Cycles (ORCs) are known to be a good alternative for the recovery pf waste heat. Among the wide variety of working fluids, refrigerants, in particular fluorinated hydrocarbons, have a great potential to increase the thermodynamic performance of these cycles.

Within the SAFT-γ Mie approach, functional groups present in HFCs have been developed, obtaining an estimation of the vapour pressure and the saturated-liquid density with an absolute average deviation (AAD), with respect to experimental data, of 3.17% and 1.77%, respectively.

Finally, once the thermodynamic model with the SAFT-γ Mie approach is developed and the transport properties are analysed, a computer-aided molecular and process design (CAMPD) framework is proposed, with the objective of maxims the power output, modifying both the working fluid and the operating conditions.

Keywords

UNIVERSITY OF VALLADOLID

SCHOOL OF INDUSTRIAL ENGINEERING

Master in Chemical Engineering

IMPERIAL COLLEGE LONDON

CHEMICAL ENGINEERING DEPARTMENT

Molecular Systems Engineering

MASTER'S THESIS

Development of a SAFT-γ Mie group-contribution approach to modelling working fluids and its application in the computer-aided molecular and process design of ORCs

Author: Jaime Santiuste Martínez

Supervisors: Andrew J. Haslam

Amparo Galindo

Rafael Mato Chaín

London, July 2020

Abstract

Organic Rankine Cycles (ORCs) are known to be a good alternative for the recovery of waste heat. Among the wide variety of working fluids, refrigerants, in particular fluorinated hydrocarbons, have a great potential to increase the thermodynamic performance of these cycles. Group-contribution (GC) approaches present a great opportunity to screen a wide variety of molecules.

Hydrofluorocarbon functional groups are developed for use within the SAFT-γ Mie approach, leading to absolute average deviations for the vapour pressure and the saturated liquid density of 3.17% and 1.77%, respectively, across a wide range of fluorinated hydrocarbon fluids collectively incorporating all of these groups. The model prediction of calorific and thermodynamic properties is analysed, obtaining a suitable description of the groups present in the molecules of interest to model thermodynamic cycles, in particular ORCs. To complete the working-fluid modelling, transport-property GC correlations are analysed for use within the ORC model developed. Finally, an outer approximation (OA) algorithm is proposed to solve the mixed integer nonlinear programming (MINLP) optimisation of the ORC, in order to obtain the optimal working fluid.

The proposed parameters for the SAFT-γ Mie groups, along with the transport-property methods, allow a complete description of the working fluid, as used in the ORC model. A computer-aided molecular and process design (CAMPD) framework is proposed, in which the solver selects the groups present in the working fluid, and then optimises the process variables in order to maximise the power output.

Abstract

Index

Summary/Objectives

Fluorinated hydrocarbons are widely used as refrigerants, working fluids for air-cooling systems or to obtain surfactants. The have also proved to be useful to increase the efficiency of power cycles like Organic Rankine Cycles, ORCs. The aim of this work is to develop a valid approach, using the SAFT-γ Mie equation of state[1–3], to model and predict the behaviour of the compounds of this family. Like other group contribution EoS, experimental data, specifically vapour pressure and saturated-liquid density, are used in a fitting procedure to refine the parameters employed.

Thermodynamic properties, mainly enthalpy and entropy, are obtained by calculating the Helmholtz free energy with the SAFT-γ Mie approach. The performance of the previously estimated parameters of the main functional groups present in fluorinated hydrocarbons is afterwards analysed to ensure an adequate estimation of these properties.

ORCs are modelled incorporating the SAFT-γ Mie approach to obtain the thermodynamic efficiency of the cycle as a function of both the set of operating conditions and the working fluid employed. This particular power cycle operates via the following stages: compression of the liquid; evaporation; expansion and condensation back to liquid phase. The operating conditions referred to previously are the operating pressures, the pinch temperature and the superheat extent. The main parameter used to rank the performance is the net power output of the cycle.

In addition to the thermodynamic properties of the hydrofluorocarbons, other properties are used during the modelling of the power cycle. In order to estimate the sizing of the cycle equipment, just like the cost estimation, properties like surface tension, viscosity or thermal conductivity are needed. To follow a similar method as for the thermodynamic properties estimated with SAFT, group-contribution correlations or methods are found to estimate transport properties.

Once the ORC cycle is modelled and the working-fluid thermodynamic and transport model is tested, a simultaneous molecular design of the working fluid and process optimisation can be carried out, establishing the framework for the Computer-Aided Molecular and Process Design (CAMPD) of the Organic Rankine Cycle (ORC). The solution of the optimisation problem comprises the optimal operating conditions, along with the optimal working fluid, defined as the addition of the functional groups proposed.

Objectives of the current work:

- Development of new functional groups within the SAFT-γ Mie approach
- Analysis of thermophysical properties GC correlations/methods
- Organic Rankine Cycle (ORC) modelling
- Computer-Aided Molecular and Process Design (CAMPD) analysis

Key words

Group contribution, SAFT-γ Mie, hydrofluorocarbons (HFCs), parameter estimation, ORC, CAMPD

1. Introduction

Hydrofluorocarbons (HFCs) are a class of organic molecule used in the refrigerants industry, to replace chlorofluorocarbons (CFCs) due to their lower ozone depletion impact. Nevertheless, it should be taken into account their high global-warming potential (GWP) compared to other working fluids. HFCs are also used in the surfactants industry, as solvents, as well as working fluids for other processes due to their low reactivity, making them suitable for use in closed cycles, reducing the corrosion of the equipment.

In order to model fluid, a wide variety of equations of state, EoS, and methods have been proposed over the years. Those fluids made of simple molecules, in which the main intermolecular forces are van der Waals attraction, like hydrocarbons, simple organic molecules or simple organics, can be modelled with engineering EoS, like Soave-Redlich-Kwong[4] or Peng-Robinson[5], corresponding states theories, group contribution approaches, etc. These equations are adequate to represent the behaviour properly for simple compounds. The problem appears when modelling complex fluids comprising strong electrolytes, polar compounds, hydrogen bonding, polymers and so on. Simple methods fail to predict the thermodynamic properties when either Coulombic, strong polar or associating forces are present. Halogenated hydrocarbons, the molecules of interest in the current work, fall into this category, as the presence of fluorine atoms increase the partial polarity of the groups forming the molecules. More-complex methods are needed to describe these strong forces. On the one hand, the quasi-chemical theory based methods, like Non-Random Two-Liquid model (NRTL)[6], the Universal Quasi-Chemical approach (UNIQUAC)[7] or the Universal Functional Activity Coefficient approach (UNIFAC)[8], force energy parameters to have larger values to capture the association interaction[9]. On the other hand, approaches based on statistical-mechanical perturbation theory have appeared in recent decades; foremost among these is the Statistical Associating Fluid Theory (SAFT)[10,11].

An important class of methods is that of the so-called group-contribution (GC) methods. These methods reduce molecules to a number of different functional groups, that can range from single atoms to groups of atoms, and that can appear several times in the molecule. The correlations of Joback and Reid[12] are a widely used method to estimate fluid properties, like the critical point or the normal boiling point, by using the parameters published for each group. In the particular case of this work, molecules are divided at each carbon atom, including in the functional group the carbon atom and the rest of atoms bonded to it.

One of the thermodynamic families of equation of state employed nowadays is the Statistical Association Fluid Theory (SAFT), a statistical mechanical approach to model the thermodynamic behaviour of fluids. SAFT-type EoS incorporate both a chain-length contribution and a molecular-association contribution, being able to predict the behaviour of not only hydrocarbons and simple organics, but also complex molecules, electrolytes and mixtures[9]. Some of the approaches within the SAFT framework are: PC-SAFT[13], soft-SAFT[14], SAFT-VR Mie[15] and SAFT-γ Mie[1]. Among the SAFT versions, the most recent researches are focused on the group-contribution SAFT approaches, including the group-contribution methodology making these frameworks more adaptable. There is a distinction between the homonuclear and heteronuclear molecular models. The homonuclear model represents molecules as associating chains of identical spherical segments, whereas the heteronuclear model employs different types of monomeric segments to describe molecules[1].

The SAFT approach employed in the current work is SAFT-γ Mie, a group contribution approach based on a heteronuclear molecular model of fused segments that interact between each other via a Mie potential of variable attractive and repulsive ranges[3]. The Mie potential can be thought of as a generalized Lennard-Jones potential, with variable ranges for the attractive and repulsive forces (see section 2.1.1. Molecular model for details). This framework has been previously used, and parameters needed to use the SAFT-γ Mie for some functional groups have been estimated, like alkyl groups[3], alkene groups[1], aromatic groups[2] and ethers[16], among others. However, there are some remaining groups needed to predict the properties of the compounds of interest of the current work. These parameters are obtained via a by fitting procedure utilising the existing experimental data. Vapour pressure and saturated-liquid densities calculated are compared to experimental data, modifying the parameters to optimise the fitting. SAFT-γ Mie provides a simultaneous description of fluid-phase behaviour, thermodynamic properties, derivative properties (Joule-Thomson coefficient, compressibility, heat capacity or speed of sound) and excess properties of mixing. Predictions made with the described framework are analysed to ensure an adequate performance of the approach.

Waste heat among different industries varies between 20-50% of the industrial energy input, of which only around 3% is being recovered for other uses[17]. This mean a large amount of energy losses due to several reasons. There are various origins of this energetic inefficiency, such as thermodynamic limitation, equipment inefficiencies, gases from furnaces, as well as cooling water heated form processes or conductive, convective and radiative losses from equipment and heated products. Usually, waste heat is available at a low temperature, making it harder to recover with a high profit, both from economic and energetic perspectives. Power-cycle performance relies mainly on the enthalpy difference between the evaporator output, at temperatures at or above the saturation temperature, and the condenser input. As the heat employed to heat-up the working fluid in the evaporator is provided by the waste-heat source, the temperature in the evaporator output, due to thermodynamic limitation, is lower than the heat-source temperature, so the lower the heat-source temperature, the lower the pressure and temperature in the evaporator output, and, then, the lower the net power output of the cycle. It should be pointed out that the heat sink considered is the ambient due to economic necessity, so the temperature difference between evaporator and compensator will not be large. Among the solutions to this issue, on the one hand, waste heat can be reduced by improving equipment and process designs, reducing the inefficiencies. On the other hand, it can be recovered with advanced cycles with higher efficiencies. The Carnot efficiency, which represents the maximum efficiency attainable, of the cycle will be low when the temperature of the heat source is not far above that of the heat sink.

Nevertheless, waste heat will still appear, so, to cope with it, waste heat can be converted to useful heat, power or electricity[17]. It can be recovered, mainly, in the three ways described before. First of all, waste heat at low temperature can be used to preheat both, gas and liquid, process streams, as well as furnace loads, water or air, reducing the energy input to the process. As the low temperature at which the heat is available reduces the applicability of waste heat, it can be used in heat pumps, upgrading the temperature at which the heat is available to the desired temperature. The heat pump absorbs the low temperature heat and releases it at the desired heat by using external energy inputs. Along with this method it can be used in heating facilities, resulting sometimes in an economically useful alternative, rather than using fossil fuels. Finally, waste heat can be used directly to obtain electrical power, with thermoelectric and piezoelectric direct generation processes, or to obtain mechanical power, with power cycles. Among these cycles, it can be outlined the steam Rankine Cycle, a Rankine Cycle that

employs steam as the working fluid, the Organic Rankine Cycle (ORC), employing organic compounds, like hydrocarbons, ethers or hydrofluorocarbons as working fluids, and the Kalina Cycle, that employs a mixture of ammonia and water as working fluid, resulting in non-isothermal phase changes that increase the efficiency of the cycle.

Organic Rankine Cycles (ORCs) are a specific variation of Rankine cycles in which the working fluid employed is an organic compound, making these cycles more suitable to work at low temperatures of the heat source and obtaining better performance, due to the lower boiling point and higher vapour pressure of these compounds, which include alkanes, haloalkanes, isoalkanes and so on[17]. ORCs have four stages to convert the heat source into useful power working between two pressures: compression, evaporation, expansion and condensation. The cycle starts with the working fluid at the low pressure as a saturated liquid, it is compressed in the pump to the high pressure of the cycle in the compression stage, then it is heated up using the heat source, until the working fluid is completely evaporated. At this stage, the working fluid can be superheated at some extent. At the outlet of the evaporator, the working fluid is expanded until the low pressure, and finally it is condensed to the initial point. Organic working fluids also allow a more compact design of the cycle, reducing the overall cost of the power obtained, on account of their higher molecular mass compared to that of water. Nevertheless, the use of low temperature heat sources implies lower efficiencies of the cycles, even though it is useful to recover at least something instead of just disposing of the waste heat.

ORCs can be split in super-critical ORCs, when the pressure in the evaporator take values over the critical one, and sub-critical ORCs, the ones considered in the current work. This second type reduce the operating cost compared with the super-critical ORCs, but lead to lower performances. Regarding the working fluid, there is a distinction between pure and mixture ORCs, and concerning the output of the evaporator, partially and superheated cycles are defined.

One critical stage of the ORC design is the working-fluid selection. As a first step in the current work, a screening of the working fluids employed in ORC researches[18–21] was carried out to analyse which molecules, or which type of molecules are desired to employ on ORCs. In previous researches, alkanes, isoalkanes, ethers and other organics have been analysed as working fluids, obtaining a heat source inlet temperature dependence to obtain an optimal fluid. Hydrofluorocarbons present adequate properties to increase the performance of the cycle, especially those with low critical temperatures and high critical pressures[22]. Also, mixtures of alkanes have been analysed in order to obtain a higher power output taking advantage of the non-isothermal evaporation and condensation stages[19].

Further studies should be carried out to ensure that the working fluid selected is suitable to work in a closed cycle, and carries with it a low corrosion impact, a low environmental impact, low toxicity and so on.

The performance of the ORC relies heavily on the operating condition of the cycle, as well as on the working fluid employed. This means that the optimal evaporator pressure for one compound is not necessarily the optimal one for a different molecule. The solution to increase the thermodynamic efficiency of the cycle is to optimise simultaneously the working fluid employed and the operating conditions, resulting in a Computer-Aided Molecular and Process Design (CAMPD) framework. Some previous studies have been focussed on this topic of simultaneous optimisation of ORCs. For example, Bowskill et al. (2020)[18] optimised the cycle using SAFT-γ Mie to described the thermodynamic and phase behaviour of the working fluid and including

feasibility tests to select the proper working fluid; Schilling et al. (2017)[23] employed the PC-SAFT framework, optimising simultaneously the operating condition and the working fluid involved. White et al. (2018)[19] carried out the CAMPD problem, using the SAFT-γ Mie approach, and including cost estimation and sizing correlation to analyse the effect of the operating condition and the working fluid. It should be noted that ORCs performance and optimal conditions relies heavily on the heat-source specification; the optimal working fluid will depend on the heat source temperature defined, resulting in heavier molecules optimal at higher temperatures.

The CAMPD – ORC proposed in the current work follows the trend of previous researches carried out on this topic, but including new groups developed also in this work and in other recent works, increasing the searching area for the working fluid, resulting in a more complete optimisation.

Complementary to the thermodynamic modelling of the working fluid, group-contribution methods and correlations are needed to predict properties of the working fluid needed for the ORC modelling in both liquid and vapour phases. The main properties analysed in the current work are the surface tension, the dynamic viscosity and the thermal conductivity. Along with the SAFT thermodynamic EoS, the working fluid can be completely characterised for the ORC modelling adding the GC correlations for these properties. It would be advisable in the interest of finding simple GC methods, to employ at the same time the thermodynamic approach and the transport properties estimation. The main purpose of these properties is the usage of them in the equipment sizing correlation and in the cost estimation correlation[24].

```
┌──────────────────────────────────────┐
│         1. Thermodynamic properties   │
│          - Parameter estiamtion       │
│            - Model validation         │
└──────────────────────────────────────┘
                   │
                   ▼
┌──────────────────────────────────────┐
│ 2. Thermophysical properties for ORC  │
│              modelling                 │
│       - Methods/correlations selection │
│            - Model validation         │
└──────────────────────────────────────┘
                   │
┌──────────────────────────────────────┐
│              3. ORC model             │
│  - Model equations/implementation      │
│              (gPROMS)                  │
│            - Model validation         │
└──────────────────────────────────────┘
                   │
┌──────────────────────────────────────┐
│            4. ORC optimisation        │
│       - MINLP optimisation problem    │
│       - Solvers selection & validation │
│          - CAMPD ORC solution         │
└──────────────────────────────────────┘
```
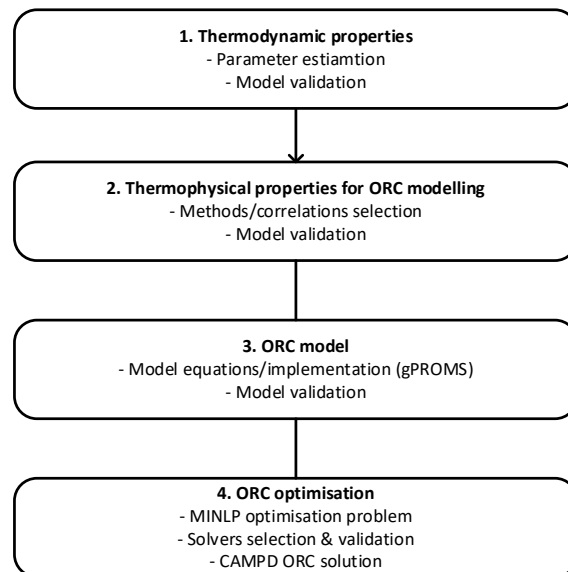
Fig. 1. Stages of the CAMPD - ORC proposed

The proposed framework includes the stages shown in Fig. 1, starting with the thermodynamic model, split into the parameter estimation and the validation of those parameters. To complete the fluid model, thermophysical properties are analysed and obtained with group-contribution methods and correlations, including the critical point prediction and the transport properties. Once the fluid model, thermodynamic and transport (Fig. 2), is analysed and validated, the ORC model is implemented and tested in order to ensure a proper estimation of the ORC behaviour. The last step is the optimisation of the ORC, obtaining the simultaneous optimal point and working fluid.
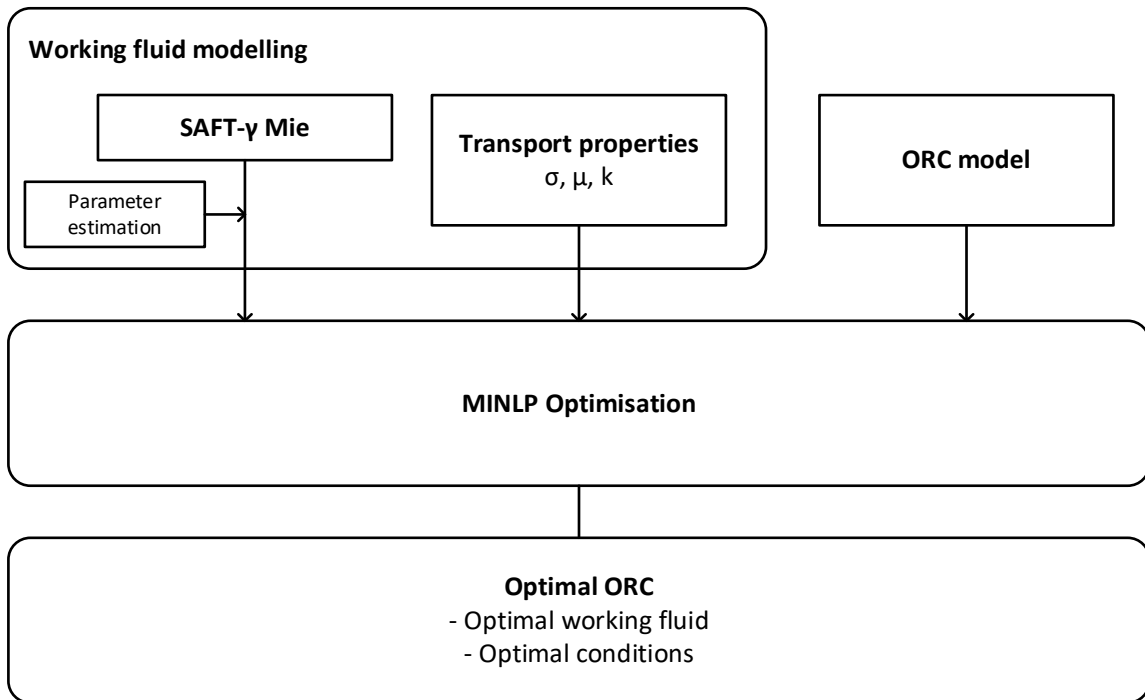
Fig. 2. Models and equations involved in the CAMPD - ORC

Within the current work, the aim is to, first of all, develop parameters of new functional groups, the ones missing to completely define hydrofluorocarbons, within the SAFT-γ Mie group contribution approach, and then to model the CAMPD – ORC framework. To reach this final model, transport properties are analysed, an ORC model is defined and implemented and, finally, the optimisation problem is defined. According to this, a parameter-estimation stage is distinguished from the ORC modelling and optimisation stage, that includes the analysis of the thermophysical properties needed for the ORC modelling.

2. Development of new functional groups

2.1. SAFT-γ Mie

The SAFT-γ Mie[3] EoS is a group contribution-approach that allows us to obtain thermodynamic properties and the phase behaviour of fluids and mixtures. This method is based on a heteronuclear molecular model, in which each molecule is defined by the functional groups present and their multiplicity. The interaction between the functional groups is modelled with Mie potentials of variable range.

2.1.1. Molecular model

As other group-contribution (GC) approaches, SAFT-γ Mie can be used to estimate a wide range of molecular properties by representing each molecule as the addition of all the functional groups and their multiplicity[3]. In this approach, molecules are divided as in Fig. 3, usually grouping together each carbon atom with the groups bounded with them. In the example shown in Fig. 3, the fused heteronuclear model for a molecule formed by four different functional groups is represented. These groups, CHF_2, CHF, CF_2 and CH_2F, have their own parameters, the combination of which leads to the final molecule characterization.

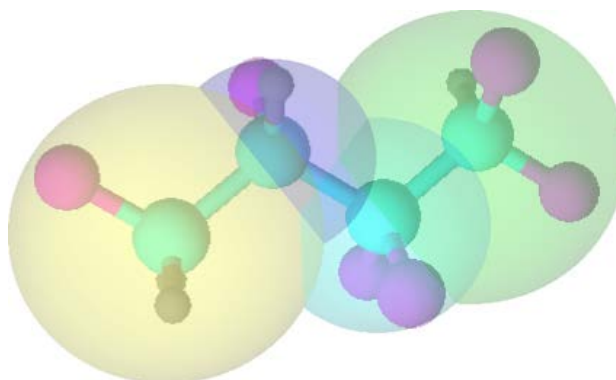*Fig. 3. Representation of a heteronuclear molecule (1,1,2,2,3,4-hexafluorobutane) within the SAFT-γ Mie approach. Cyan: carbon, black: hydrogen and Magenta: fluorine*

Additionally, SAFT-γ Mie theory includes the description of strong interaction forces, such as hydrogen bonding, by adding a number of short-range association sites placed on the segments where these forces take place.

Intermolecular potential

The intermolecular interaction between two segments, *k* and *l*, is assumed to have the form of the Mie potential[25], a generalised form of the Lennard-Jones potential. The potential of the interaction between two segments is calculated with eq. [1] as a function of the intersegment distance r_{kl}:

$$\emptyset_{kl}^{Mie}(r_{kl}) = C_{kl} \cdot \varepsilon_{kl} \cdot \left[\left(\frac{\sigma_{kl}}{r_{kl}} \right)^{\lambda_{kl}^{r}} - \left(\frac{\sigma_{kl}}{r_{kl}} \right)^{\lambda_{kl}^{a}} \right] \tag{1}$$

where $\emptyset_{kl}^{Mie}$ is the intersegment potential, ε_{kl} the depth of potential well between *k* and *l* segments, λ_{kl}^{a} and λ_{kl}^{r} are the intermolecular attractive and repulsive ranges of potential and σ_{kl} the segment diameter. The term C_{kl} the (eq.[2]) is a term to ensure a minimum potential of $-\varepsilon_{kl}$.

$$C_{kl} = \frac{\lambda_{kl}^r}{\lambda_{kl}^r - \lambda_{kl}^a} \cdot \left(\frac{\lambda_{kl}^r}{\lambda_{kl}^a}\right)^{\frac{\lambda_{kl}^a}{\lambda_{kl}^r - \lambda_{kl}^a}} \qquad [2]$$

The Mie potential is represented in Fig. 3 for the interaction of two equal segments of type k. The parameters described above are shown in the figure and its physical sense. The potential shape is similar in the case of the unlike interaction between two segments, k and l.
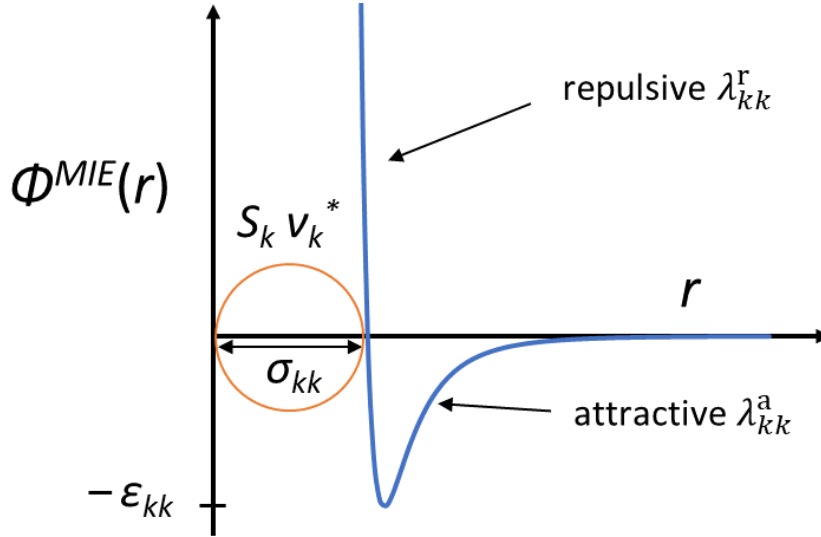

Fig. 4. Mie potentials. $\Phi^{MIE}(r)$: intermolecular potential. ε_{kk}: dispersive energy. σ_{kk}: segment diameter. S_k: shape factor. λ_{kl}^a and λ_{kl}^r : attractive and repulsive intermolecular potentials. r: intersegment distance. v_k^*: number of segments

For the association sites, like hydrogen bonding or other short-range interaction, the interaction is modelled with a square-well potential between a site of type a place on a segment of type k and a site of type b placed on a segment of type l, as described in eq. [3]:

$$\emptyset_{kl,ab}^{HB}(r_{kl,ab}) = \begin{cases} -\varepsilon_{kl,ab}^{HB} & if \ r_{kl,ab} \leq r_{kl,ab}^c, \\ 0 & if \ r_{kl,ab} > r_{kl,ab}^c, \end{cases} \qquad [3]$$

where $r_{kl,ab}$ is the centre-centre distance between both sites, $r_{kl,ab}^c$ the cut-off range of the association interaction and $\varepsilon_{kl,ab}^{HB}$ the depth of the association-energy well. The distance between the segment centre and the site centre is represented by $r_{kk,aa}^d$.

To sum up, a functional group is represented by the number of identical segments, v_k^*, the shape factor, S_k, that represents the extent to which the segment contribute to the overall molecule, the segment diameter, σ_{kk}, the attractive and repulsive ranges of potential, λ_{kk}^a and λ_{kk}^r and the energy of interaction, ε_{kk} between segments of type k. The association interaction between groups is calculated with the number of different site types, $N_{ST,k}$, the number of sites of a given type, $n_{k,a}, n_{k,b} \dots n_{k,N_{ST,k}}$, the distance between the group and the site, $r_{kk,aa}^d$, the association energy, $\varepsilon_{kk,ab}^{HB}$, the bonding volume parameter, $K_{kk,ab}$, and the cut-off range, $r_{kl,ab}^c$. In the current version of SAFT used, $r_{kk,aa}^d$ and $r_{kl,ab}^c$ are both fixed to a value of $0.4 \cdot \sigma_{kk}$. The interaction between the groups k and l is characterised by the parameters $\sigma_{kl}, \lambda_{kl}^a, \lambda_{kl}^r$ and ε_{kl}, and the association parameters $\varepsilon_{kl,ab}^{HB}$ and $K_{kl,ab}$. A system is represented in the current theory by the set $v_{k,i}$, that collects the number of groups of type k in the compound i.

2.1.2. Helmholtz free energy

As in other formal statistical-mechanical approaches, SAFT-γ Mie EoS is used to provide the Helmholtz free energy, employed to obtain the macroscopic thermodynamic properties from the molecular model, SAFT-γ Mie in the current work[1]. The expression [4] collects all the terms used to obtain the overall Helmholtz free energy A:

$$\frac{A}{Nk_BT} = \frac{A^{ideal}}{Nk_BT} + \frac{A^{mono}}{Nk_BT} + \frac{A^{chain}}{Nk_BT} + \frac{A^{assoc}}{Nk_BT} \quad [4]$$

where A^{ideal} is the ideal contribution to the free energy, A^{mono} is the attractive and repulsive Mie-segments interactions free energy, A^{chain} is the contribution to the free energy derived from the molecule formation and A^{assoc} accounts the free energy from the association interaction. N represents the total number of molecules, k_B the Boltzmann constant and T the absolute temperature. These terms are explained in detail below.

Ideal term

The ideal contribution to the Helmholtz free energy is calculated with eq. [2]:

$$\frac{A^{ideal}}{Nk_BT} = \left(\sum_{i=1}^{N_C} x_i \ln\left(\rho_i \Lambda_i^3\right) \right) - 1 \quad [5]$$

where x_i is the mole fraction of component i, $\rho_i = N_i/V$ the number density, N_i the number of molecules of component i and V the total volume of the system. Λ_i^3 represents the thermal de Broglie volume and incorporates the effects of translational, rotational and vibrational contributions to the kinetic energy. N_C refers to the total number of the components.

Monomer term

The monomer contribution to the free energy refers to the attractive and repulsive interactions characterised by the Mie potential. It is obtained using a Barker-Henderson[26] high-temperature perturbation up to third order [6],

$$\frac{A^{mono}}{Nk_BT} = \frac{A^{HS}}{Nk_BT} + \frac{A_1}{Nk_BT} + \frac{A_2}{Nk_BT} + \frac{A_3}{Nk_BT} \quad [6]$$

where the hard-sphere free energy contribution, A^{HS}, calculated with eq. [7] and the rest of terms, A_q, are obtained with eq. [10].

$$\frac{A^{HS}}{Nk_BT} = \left(\sum_{i=1}^{N_C} x_i \sum_{k=1}^{N_G} v_{k,i} v_k^* S_k \right) a^{HS} \quad [7]$$

$v_{k,i}$ is the number of groups of the type k in the compound i and a^{HS} is the dimensionless contribution to the hard-sphere free energy. This term is a function of the segment density, ρ_s, the mole fractions and the diameters of the sements[1]

$$\rho_s = \rho \left(\sum_{i=1}^{N_C} x_i \sum_{k=1}^{N_G} v_{k,i} v_k^* S_k \right) \quad [8]$$

$x_{s,k}$ is the fraction of segments of a group of type k in the mixture, calculated with eq. [9]:

$$x_{s,k} = \frac{\sum_{i=1}^{N_C} x_i \nu_{k,i} \nu_k^* S_k}{\sum_{j=1}^{N_C} x_j \sum_{l=1}^{N_G} \nu_{l,j} \nu_l^* S_l} \qquad [9]$$

The rest of the terms from eq. [6], A_q, are obtained from eq. [10]:

$$\frac{A_q}{N k_B T} = \left(\frac{1}{k_B T}\right) \left(\sum_{i=1}^{N_C} x_i \sum_{k=1}^{N_G} \nu_{k,i} \nu_k^* S_k\right) a_q \qquad q = 1, 2, 3 \qquad [10]$$

where a_q is the dimensionless contribution to the free energy,

$$a_q = \sum_{k=1}^{N_G} \sum_{l=1}^{N_G} x_{s,k} x_{s,l} a_{q,kl} \qquad q = 1, 2, 3 \qquad [11]$$

Chain term

The Helmholtz free energy contribution for the formation of molecules, A^{chain}, is obtained with eq. [12],

$$\frac{A^{chain}}{N k_B T} = -\sum_{i=1}^{N_C} x_i \left(\sum_{k=1}^{N_G} \nu_{k,i} \nu_k^* S_k - 1\right) \cdot \ln g_{ii}^{Mie}(\bar{\sigma}_{ii}; \zeta_x) \qquad [12]$$

where ζ_x is the packaging fraction of a hypothetical fluid, calculated with eq. [18], and $g_{ii}^{Mie}(\bar{\sigma}_{ii}; \zeta_x)$ the value of the RDF, at a distance $\bar{\sigma}_{ii}$, calculated in eq. [19].

The molecular fraction of a group k in a molecule i, $z_{k,i}$ is obtained with eq. [13].

$$z_{k,i} = \frac{\nu_{k,i} \nu_k^* S_k}{\sum_{l=1}^{N_G} \nu_{l,i} \nu_l^* S_l} \qquad [13]$$

The chain free energy contribution is obtained using average molecular parameters, $\bar{\sigma}_{ii}$, $\bar{d}_{ii}$, $\bar{\varepsilon}_{ii}$ and $\bar{\lambda}_{ii}$, calculated with the following equations.

$$\bar{\sigma}_{ii}^3 = \sum_{k=1}^{N_G} \sum_{l=1}^{N_G} z_{k,i} z_{l,i} \bar{\sigma}_{kl}^3 \qquad [14]$$

$$\bar{d}_{ii}^3 = \sum_{k=1}^{N_G} \sum_{l=1}^{N_G} z_{k,i} z_{l,i} \bar{d}_{kl}^3 \qquad [15]$$

$$\bar{\varepsilon}_{ii} = \sum_{k=1}^{N_G} \sum_{l=1}^{N_G} z_{k,i} z_{l,i} \bar{\varepsilon}_{kl} \qquad [16]$$

$$\bar{\lambda}_{ii} = \sum_{k=1}^{N_G} \sum_{l=1}^{N_G} z_{k,i} z_{l,i} \bar{\lambda}_{kl} \qquad [17]$$

The packing fraction of a hypothetical fluid of diameter $d_x^3 = \sum_{k=1}^{N_G} \sum_{l=1}^{N_G} x_{s,k} x_{s,l} d_{k,l}^3$ is obtained by:

$$\zeta_x = \frac{\pi \rho_s}{6} \sum_{k=1}^{N_G} \sum_{l=1}^{N_G} x_{s,k} x_{s,l} d_{kl}^3 \qquad [18]$$

The RDF used is a second-order expansion,

$$g_{ii}^{Mie}(\bar{\sigma}_{ii};\zeta_x) = g_d^{HS}(\bar{\sigma}_{ii};\zeta_x) \exp\left(\frac{\beta\,\bar{\varepsilon}_{ii}\,g_1(\bar{\sigma}_{ii})}{g_d^{HS}(\bar{\sigma}_{ii};\zeta_x)} + \frac{(\beta\,\bar{\varepsilon}_{ii})^2\,g_2(\bar{\sigma}_{ii})}{g_d^{HS}(\bar{\sigma}_{ii};\zeta_x)}\right) \qquad [19]$$

where $g_d^{HS}(\bar{\sigma}_{ii};\zeta_x)$ is the RDF of a system of hard spheres of diameter $\bar{d}_{ii}$ evaluated at a distance $\bar{\sigma}_{ii}$ and a packing fraction of ζ_x. The RDF terms are approximated ([20]) by the value at the contact distance $\bar{d}_{ii}$,

$$g_q(\bar{\sigma}_{ii}) \approx g_q(\bar{d}_{ii}) \qquad q = 1,2 \qquad [20]$$

Association term

The association interaction of molecules due to the definition of bonding sites is calculated with eq. [21], following the Wertheim TPT1 form[27], summing over the number of compounds, N_C, the number of groups, N_G, and over the number of site types on each group, $N_{ST,k}$:

$$\frac{A^{assoc}}{Nk_BT} = \sum_{i=1}^{N_C} x_i \sum_{k=1}^{N_G} v_{k,i} \sum_{a=1}^{N_{ST,k}} n_{k,a}\left(ln\,X_{i,k,a} + \frac{1 - X_{i,k,a}}{2}\right) \qquad [21]$$

where $n_{k,a}$ is the number of sites of type a on a group k and $X_{i,k,a}$ the fraction of molecules of component i that are not bonded at a site a on group k, calculated with eq. [22]:

$$X_{i,k,a} = \left[1 + \rho \sum_{j=1}^{N_C} x_j \sum_{l=1}^{N\_G} v_{l,j} \sum_{b=1}^{N_{ST,l}} n_{l,b} X_{j,l,b} \Delta_{ij,kl,ab}\right]^{-1} \qquad [22]$$

where $\Delta_{ij,kl,ab}$ means the overall strength of association between a site of type a on a group k of component i and a site of type b on a group l of component j, obtained with eq. [23]

$$\Delta_{ij,kl,ab} = F_{kl,ab} K_{kl,ab} I_{ij,kl,ab} \qquad [23]$$

where $F_{kl,ab}$ is calculated with eq. [24], the temperature-density polynomial correlation of the association integral, $I_{ij,kl,ab}$, is obtained from eq. [25] and $K_{kl,ab}$ is the bonding volume parameter.

$$F_{kl,ab} = \exp\left(\frac{\varepsilon_{kl,ab}^{HB}}{k_BT}\right) - 1 \qquad [24]$$

$$I_{ij,kl,ab} = \sum_{p=0}^{10} \sum_{q=0}^{10-p} c_{pq}(\rho_s\sigma_x^3)\left(\frac{k_BT}{\bar{\varepsilon}_{ij}}\right)^q \qquad [25]$$

c_{pq} are coefficients obtained from bibliography[28], and parameters σ_x^3, $\bar{\varepsilon}_{ij}$ and $\bar{\sigma}_{ij}$ are obtained using the following equations.

$$\sigma_x^3 = \sum_{k=1}^{N_G} \sum_{l=1}^{N_G} x_{s,k} x_{s,l} \sigma_{kl}^3 \qquad [26]$$

$$\bar{\varepsilon}_{ij} = \frac{\sqrt{\bar{\sigma}_{ii}^3 \bar{\sigma}_{jj}^3}}{\bar{\sigma}_{ij}} \sqrt{\bar{\varepsilon}_{ii}\bar{\varepsilon}_{jj}} \qquad [27]$$

$$\bar{\sigma}_{ij} = \frac{\bar{\sigma}_{ii} + \bar{\sigma}_{jj}}{2} \qquad [28]$$

2.1.3. Combining rules

As well as the self-interaction parameters, in order to use the described method, the unlike intermolecular interaction parameters are required. To obtain the unlike parameters, combing rules that described the parameters as a function of the self-interaction parameters of the two functional groups are used when possible. These relations are commonly used to facilitate the estimation of binary or mixtures behaviour, without having to optimise all the cross-interaction parameters[3].

These combining rules are described below, in eq. [10-15]. Each intermolecular parameter is calculated as a combination of the functional-group parameters.

The unlike segment diameter, σ_{kl}, is calculated following eq. [29] by a simple arithmetic mean of the self-interaction segment diameters of groups k and l[3].

$$\sigma_{kl} = \frac{\sigma_{kk} + \sigma_{ll}}{2} \qquad [29]$$

An arithmetic mean is also used in eq. [30] to obtain the unlike Barker-Henderson hard-sphere diameter, d_{kl}, instead of using the more-rigorous approach of the numerical integration of the segment diameter, reducing the computational cost[1].

$$d_{kl} = \frac{d_{kk} + d_{ll}}{2} \qquad [30]$$

The unlike dispersive energy, ε_{kl}, is obtained by using an augmented geometric mean [31][1].

$$\varepsilon_{kl} = \frac{\sqrt{\sigma_{kk}^3 \sigma_{ll}^3}}{\sigma_{kl}^3} \sqrt{\varepsilon_{kk} \varepsilon_{ll}} \qquad [31]$$

The combining rule for both, the attractive and repulsive ranges of potential, λ_{kl}^a and λ_{kl}^r, is described in eq. [32][1].

$$\lambda_{kl} = 3 + \sqrt{(\lambda_{kk} - 3)(\lambda_{ll} - 3)} \qquad [32]$$

In the case of the association parameters, eq. [33] collects the combining rule for the unlike association energy, $\varepsilon_{kl,ab}^{HB}$, as a geometric mean, and eq. [34] the one for the unlike volume bonding, $K_{kl,ab}$[1].

$$\varepsilon_{kl,ab}^{HB} = \sqrt{\varepsilon_{kk,aa}^{HB} \varepsilon_{ll,bb}^{HB}} \qquad [33]$$

$$K_{kl,ab} = \left(\frac{\sqrt[3]{K_{kk,aa}} + \sqrt[3]{K_{ll,bb}}}{2} \right)^3 \qquad [34]$$

2.1.4. Functional groups

The SAFT-γ Mie equation of state is a group-contribution approach in which the fluids are represented by their functionals groups and the interactions between them.

For the main objective of the project, the functional groups of interest are collected in Table 1. In that table, group interaction parameters are represented in each cell, where the group on the left is the *k* group, and the group on the top is the *l* group. When *k* and *l* are different functional

groups, the cell represents the unlike interaction, whereas when both groups are the same, the self-interaction is represented. The ones that appear with the reference are those which has been previously estimated and the ones with the x refer to those that are estimated in the current work. CR refers to the use of combining rules to estimate the value of the parameters instead of optimising the parameters themselves by fitting them to experimental data.

*Table 1. Summary of the functional groups and the unlike interactions used in the current work. Each cell represents the group-group interaction parameters. CR: combining rule. *: to be published. x: estimated in the current work.*

	CH₃	CH₂	CH₂F	CHF₂	CHF	CF₃	CF₂
CH₃	3						
CH₂	3	3					
CH₂F	x	x	x				
CHF₂	x	x	x	x			
CHF	x	x	x	x	x		
CF₃	x	x	x	x	x	*	
CF₂	x	x	x	x	CR	*	*

As a reminder, each functional group of a molecule is defined by the following parameters, the number of segments, ν_k^*, the shape factor, S_k, the segment diameter, σ_{kk}, the attractive and repulsive ranges of potential, λ_{kk}^a and λ_{kk}^r, and the like dispersive energy, ε_{kk}. Like parameters of the alkyl and perfluoroalkyl functional groups are collected in Table 2 . The attractive range of potential, λ_{kk}^a, is assigned to London-dispersion value of 6 for every functional group.

*Table 2. Like group parameters for use within the SAFT-γ Mie group-contribution approach. *: to be published*

k	Group k	ν_k^*	S_k	λ_{kk}^r	λ_{kk}^a	σ_{kk} /Å	(ε_{kk}/k_B) /K	Ref.
1	CH₃	1	0.57255	15.050	6.0000	4.0772	256.777	3
2	CH₂	1	0.22932	19.871	6.0000	4.8801	473.39	3
3	CF₃	1	0.54490	28.904	6.0000	4.9310	325.00	*
4	CF₂	1	0.27520	33.963	6.0000	5.1980	459.92	*

The unlike interaction between two functional groups is represented by the unlike segment diameter, σ_{kl}, the attractive and repulsive range of potential, λ_{kl}^r, the unlike dispersive energy, ε_{kl}. The unlike interaction group parameters are collected in Table 3, whereas the rest of parameters are obtained by the combining rules [equation].

*Table 3. Unlike group interaction parameters for use within the SAFT- γ Mie group-contribution approach. *: to be published*

k	l	Group k	Group l	(ε_{kl}/k_B)/ K	Ref.
1	2	CH₃	CH₂	350.77	3
3	4	CF₃	CF₂	390.00	*

The remaining parameters are estimated in the current work. When all the parameters of Table 1 are estimated, the group contribution approach can be used for all the possible molecules involving the mentioned groups.

2.1.5. Parameter estimation

Within the SAFT-γ Mie equation of state, molecules are defined by their functional groups, characterised by their parameters and the interaction between them. Parameters for the alkyl and perfluoroalkyl have been obtained in previous works (Table 2). The remaining functional groups are characterised in the current work, following the next methodology[2,3].

A functional group is represented by the parameters cited in the section 2.1.1. Molecular model. The unlike interaction is obtained by the combining rules, summarised in section 2.1.3. Combining rules, involving the like parameters of the functional groups, except for the unlike dispersive energy, ε_{kl}. The number of segments, v_k^*, is set to 1 for all the groups in the current work. To sum up, the following parameters have been estimated with this methodology: the shape factor, S_k, the segment diameter, σ_{kk}, the attractive and repulsive ranges of potential, λ_{kk}^a and λ_{kk}^r, the like dispersive energy, ε_{kk}, and the unlike dispersive energy, ε_{kl}.

These parameters of the functional groups of interest are estimated. To do so, experimental data are compared with the group contribution approach results, and the difference between both is minimised varying the parameters considered for the estimation. The experimental data of interest for parameter estimation have proved to be VLE (Vapour-liquid equilibrium) data[3], and more precisely, the vapour pressure, p_{vap}, and the saturated liquid density, ρ_{liq}^{sat}. In the case of experimental data from binary mixtures, that are used in the case that no pure experimental data are available, bubble pressure, p_{Bubble}, and dew pressure, p_{Dew}, are used to obtain the parameters.

The experimental data and the model data are compared using the equation [35], that sets the objective function to minimise in order to reduce the error between the SAFT model, with the parameters to optimise, and the experimental data gathered. This objective function is the result of the weighted addition of the square of the relative error in the vapour pressure and the square of the relative error in the saturation liquid density[3]. Variables ω_1 and ω_2 represent the weights of each property in the final function. In this particular case, both weights are assigned the value of $\omega_1 = \omega_2 = 1$, so both properties have equal weighting in the objective function.

$$
\begin{aligned}
\min_{\Omega} f_{obj} = \omega_1 & \sum_m^{N_{P_{vap}}} \left[\frac{p_{vap}^{exp}(T_m) - p_{vap}^{calc}(T_m, \Omega)}{P_{vap}^{exp}(T_m)} \right]^2 \\
+ \omega_2 & \sum_n^{N_{\rho_{l,sat}}} \left[\frac{\rho_{L,sat}^{exp}(T_n) - \rho_{L,sat}^{calc}(T_n, \Omega)}{\rho_{l,sat}^{exp}(T_n)} \right]^2
\end{aligned}
\tag{35}
$$

When the experimental data used to estimate the functional groups are binary VLE data equation [36] is used instead. The objective function to minimise in this case is the addition of the relative error between both, the experimental and calculated dew and bubble pressure.

$$
\begin{aligned}
\min_{\Omega} f_{obj} = \omega_1 & \sum_m^{N_{P_{bubble}}} \left[\frac{P_{Bubble}^{exp}(T_m, n) - P_{Bubble}^{calc}(T_m, n, \Omega)}{P_{Bubble}^{exp}(T_m, n)} \right]^2 \\
+ \omega_2 & \sum_n^{N_{P_{Dew}}} \left[\frac{P_{Dew}^{exp}(T_n, n) - P_{Dew}^{calc}(T_n, n, \Omega)}{P_{Dew}^{exp}(T_n, n)} \right]^2
\end{aligned}
\tag{36}
$$

The variable Ω (present in equations [35] and [36]) represents the vector of parameters that are going to be estimated by minimising the objective function. This set of parameters could belong

only to one functional group or to a wide range of groups. Furthermore, this set could include only self-interaction parameters, only unlike interaction parameters or both of them.

Once the parameters to estimate are selected, upper and lower bounds are set, so the parameters obtained drop into the feasible range. The resulting problem is a NonLinear Problem, NLP, in which function [35], or [36] in case a binary system is used, is minimised modifying the set of parameters Ω, that is bounded by Ω^L and Ω^U. The NLP solver used belongs to the category of multiple-starting-points solvers, in which a Sobol sequence is used to specify the initial guess of the parameters estimated in each step. The software used in this step is python, and more precisely gSAFTmm[29], a compiled version of SAFT-γ Mie.

Experimental data

The experimental data selection was carried out taking into account the presence of the functional groups to be estimated, and also the absence of other functional groups or interactions not available in the literature, reducing the parameters to estimate to the ones identified previously as the relevant ones for the current work.

The compounds used belong to the category of refrigerants, and were selected from a wide range of molecules, using the experimental data availability, of the selected properties, and the quality of the data as the factors to decide which set of experimental data employ in the current work. In Table 4 the experimental data used in the parameter optimisation are summarised, including the compound, the temperature range, and number of points for both properties of interest.

According to previous work[3], in order to obtain the more accurate parameters to use this group contribution approach, the VLE experimental data used in the estimation process should cover the range from the triple point to 90% of the critical temperature of the fluid. This criterion has been used in the current work to obtain the desired parameters. The main reason of avoiding experimental data near the critical region is to prevent the possible loss of the physical significance of the parameters due to an improvement of the critical region description. It has been proved that, for an analytical equation of state, is not possible to capture at the same time both the critical and the subcritical regions accurately. For this reason, experimental data employed are limited to 90% of the critical temperature, ensuring an adequate model for the subcritical region.

A summary of the compound used in this process, as well as the temperature range of the data available and the number of points, for both properties employed, the pure vapour pressure and the liquid saturation density is represented in Table 4.

Experimental data from only one mixture, 1,1,1,2-tetrafluoroethane (R-134a) and 1,1,1,2,3,3,3-heptafluoropropane (R-227ea)[30], were used in the current parameter optimisation.

Table 4. Experimental data of pure refrigerants. T_{TP}: triple point temperature. T_{cr}: critical point temperature. T range: range of temperatures of the experimental data employed. n: number of experimental points. Ref.: bibliography reference of the experimental data.

Name	Molecular Formula	T_{TP} /K	T_{cr} /K	Vap. Pressure			Density		
				T range /K	n	Ref.	T range /K	n	Ref.
Pentafluoroethane	C_2HF_5	172.52	339.26	223 - 303	29	[31]	248 - 306	16	
1,1,2,2-tetrafluoroethane	$C_2H_2F_4$	120.00	391.85	150 - 350	21	[32]	150 - 350	21	[32]
1,1,1,2-tetrafluoroethane	$C_2H_2F_4$	169.85	374.07	204 - 333	34	[33]	253 - 333	18	[34]
1,1,2-trifluoroethane	$C_2H_3F_3$	189.20	425.00	220 - 380	15	[32]	314 - 378	13	[35]
1,1,1-trifluoroethane	$C_2H_3F_3$	161.00	346.25	251 - 311	31	[36]	230 - 310	13	[37]
1,1-difluoroethane	$C_2H_4F_2$	150.00	386.50	243 - 343	54	[38]	243 - 343	26	[38]
Fluoroethane	C_2H_5F	130.00	375.00	180 - 330	16	[32]	180 - 340	17	[32]
1,1,1,2,3,3,3-heptafluoropropane	C_3HF_7	146.35	375.04	233 - 338	54	[39]	243 - 337	38	[40]
1,1,1,2,3,3-hexafluoropropane	$C_3H_2F_6$	242.00	412.21	293 - 363	17	[41]	262 - 343	37	[42]
1,1,1,3,3,3-hexafluoropropane	$C_3H_2F_6$	179.52	398.07	271 - 359	68	[39]	262 - 353	38	[42]
1,1,2,2,3-pentafluoropropane	$C_3H_3F_5$	200.00	447.57	250 - 400	16	[32]	200 - 400	21	[32]
1,1,1,2,2-pentafluoropropane	$C_3H_3F_5$	120.00	381.65	280 - 343	14	[43]	296 - 344	6	[43]
1,1,1,3,3-pentafluoropropane	$C_3H_3F_5$	171.05	430.65	235 - 386	101	[39]	250 - 314	65	[44]
1-fluoropropane	$C_5H_{11}F$	130.00	419.00	230 - 370	15	[32]	200 - 370	18	[32]
2-Fluoropropane	C_3H_7F	130.00	410.40	230 - 370	15	[32]	200 - 370	18	[32]
1,1,1,2,2,3,3,4,4-nonafluorobutane	C_4HF_9	130.00	413.00	270 - 370	11	[32]	298 - 373	6	[43]
1,1,1,2,2,3,3,4-octafluorobutane	$C_4H_2F_8$	130.00	433.65	260 - 390	14	[32]	200 - 390	20	[32]
1,1,1,3,3-pentafluorobutane	$C_4H_5F_5$	239.00	459.91	298 - 413	20	[45]	289 - 413	8	[45]
2-fluorobutane	C_4H_9F	140.00	448.00	216 - 298	6	[46]	200 - 400	21	[32]
1-fluoropentane	C_3H_7F	150.00	496.70	300 - 440	15	[32]	200 - 440	25	[32]

2.2. Results and discussion

2.2.1. Parameter estimation

Some of the groups of interest for the current work have not been studied under the SAFT-γ Mie approach. As summarised previously, to use this group-contribution approach, like and unlike interaction parameters are needed, so VLE and other properties of interest can be predicted.

To obtain these parameters, the method proposed in 2.1.5. Parameter estimation is employed, minimising the deviation between the experimental and calculated data for the vapour pressure and saturated-liquid density, for pure compounds, and dew and bubble pressure for the binary mixture. The parameters estimated are those considered in the method section as the ones needed to describe the behaviour of the desired compounds.

The experimental data collected allows the calculation of the necessary parameters to use the selected EoS to simulate ORCs. However, there are experimental data published only for a reduced number of refrigerants. For this reason, all the experimental data available are used in the estimation, neglecting the validation step, that consists of predicting the VLE for the remaining molecules.

The steps followed with this purpose are summarised in Fig. 5. First of all, starting with the already known groups, the alkyl and perfluoroalkyl groups, in the first step, the unlike interaction between these groups is estimated. In the second step, the parameters to describe the group CHF_2 are estimated, including the self-interaction and the unlike interactions with the previously obtained groups. The third step is defined to obtain the functional group CH_2F with its unlike parameters with the rest of groups previously estimated in the current work or in the bibliography. The last step, the fourth, describes the CHF group. In this step the unlike interaction between CHF and CF_2 is not estimated and the dispersive energy is obtained with a combining rule (CR).
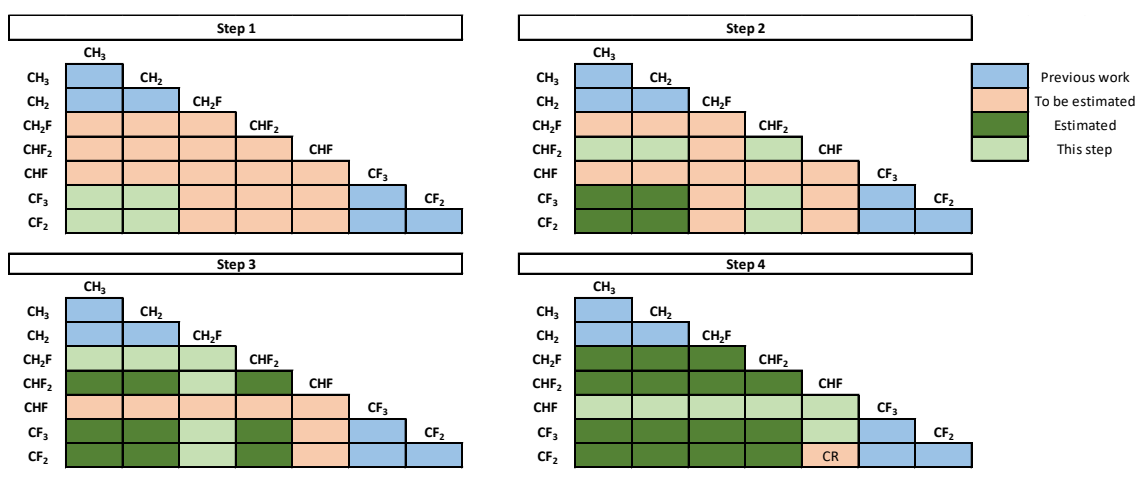

Fig. 5. Parameters estimated at each step of the parameter estimation. CR: combining rule employed to estimate the unlike parameter. Each cell represents the group-group interaction parameters.

The compounds, and their experimental data, used at each step described above are collected in Table 5. Additionally, the functional groups multiplicity is attached to each molecule.

Table 5. Experimental data used at each step of the parameter estimation. The groups columns represent the multiplicity of each of the employed functional groups present in each compound.

Step	Compound	Molecular formula	CH₃	CH₂	CH₂F	CHF₂	CHF	CF₃	CF₂
1	1,1,1-trifluoroethane	$C_2H_3F_3$	1	-	-	-	-	1	-
	1,1,1,3,3,3-hexafluoropropane	$C_3H_2F_6$	-	1	-	-	-	2	-
	1,1,1,2,2-pentafluoropropane	$C_3H_3F_5$	1	-	-	-	-	1	1
	1,1,1,3,3-pentafluorobutane	$C_4H_5F_5$	1	1	-	-	-	1	1
2	Pentafluoroethane	C_2HF_5	-	-	-	1	-	1	-
	1,1,2,2-tetrafluoroethane	$C_2H_2F_4$	-	-	-	2	-	-	-
	1,1-difluoroethane	$C_2H_4F_2$	1	-	-	1	-	-	-
	1,1,1,3,3-pentafluoropropane	$C_3H_3F_5$	-	1	-	1	-	1	-
	1,1,1,2,2,3,3,4,4-nonafluorobutane	C_4HF_9	-	-	-	1	-	1	2
3	1,1,1,2-tetrafluoroethane	$C_2H_2F_4$	-	-	1	-	-	1	-
	1,1,2-trifluoroethane	$C_2H_3F_3$	-	-	1	1	-	-	-
	Fluoroethane	C_2H_5F	1	-	1	-	-	-	-
	1,1,2,2,3-pentafluoropropane	$C_3H_3F_5$	-	-	1	1	-	-	1
	1-fluoropropane	$C_5H_{11}F$	1	1	1	-	-	-	-
	1,1,1,2,2,3,3,4-octafluorobutane	$C_4H_2F_8$	-	-	1	-	-	1	2
	1-fluoropentane	C_3H_7F	1	3	1	-	-	-	-
4	1,1,1,2,3,3,3-heptafluoropropane	C_3HF_7	-	-	-	-	1	2	-
	1,1,1,2,3,3-hexafluoropropane	$C_3H_2F_6$	-	-	-	1	1	1	-
	2-Fluoropropane	C_3H_7F	2	-	-	-	1	-	-
	2-fluorobutane	C_4H_9F	2	1	-	-	1	-	-

The parameters obtained are collected in two tables, the self-interaction parameters in Table 6 and the unlike parameters for all the possible combinations in Table 7.

*Table 6. Like group parameters for use within the SAFT-γ Mie group-contribution approach. *: reference to be published. cw: current work*

k	Group k	v_k^*	S_k	λ_{kk}^r	λ_{kk}^a	σ_{kk} /Å	(ε_{kk}/k_B)/ K	Ref.
1	CH₃	1	0.57255	15.050	6.0000	4.0772	256.777	[1]
2	CH₂	1	0.22932	19.871	6.0000	4.8801	473.39	[1]
3	CF₃	1	0.54490	28.904	6.0000	4.9310	325.00	*
4	CF₂	1	0.27520	33.963	6.0000	5.1980	459.92	*
5	CH₂F	1	0.86762	22.340	6.0000	3.7127	503.86	cw
6	CHF₂	1	0.95981	19.294	6.0000	3.7006	298.15	cw
7	CHF	1	0.42617	33.025	6.0000	4.2010	346.13	cw

*Table 7. Unlike group interaction parameters for use within the SAFT- γ Mie group-contribution approach. *: reference to be published. cw: current work*

k	l	Group k	Group l	(ε_{kl}/k_B)/ K	Ref.
1	2	CH$_3$	CH$_2$	350.77	[1]
1	3	CH$_3$	CF$_3$	412.05	cw
1	4	CH$_3$	CF$_2$	329.38	cw
1	5	CH$_3$	CH$_2$F	228.75	cw
1	6	CH$_3$	CHF$_2$	354.13	cw
1	7	CH$_3$	CHF	438.02	cw
2	3	CH$_2$	CF$_3$	586.50	cw
2	4	CH$_2$	CF$_2$	757.58	cw
2	5	CH$_2$	CH$_2$F	382.05	cw
2	6	CH$_2$	CHF$_2$	405.80	cw
2	7	CH$_2$	CHF	469.93	cw
3	4	CF$_3$	CF$_2$	390.00	*
3	5	CF$_3$	CH$_2$F	319.42	cw
3	6	CF$_3$	CHF$_2$	317.06	cw
3	7	CF$_3$	CHF	448.14	cw
4	5	CF$_2$	CH$_2$F	377.72	cw
4	6	CF$_2$	CHF$_2$	325.87	cw
4	7	CF$_2$	CHF	CR	cw
5	6	CH$_2$F	CHF$_2$	307.41	cw
5	7	CH$_2$F	CHF	570.70	cw
6	7	CHF$_2$	CHF	398.14	cw

It is noted that for the unlike interaction of CF$_2$ and CHF, the use of a combining rule [31] is proposed to estimate the dispersive energy. The main reason for this is the lack of experimental data, either pure or mixture data, containing both groups.

Vapour pressure

The vapour pressure of pure refrigerants is used to estimate the unknown parameters. To evaluate the accuracy of the proposed approach, the vapour pressure calculated with the current method is plotted along with the experimental data collected of those refrigerants used in the parameter estimation stage, as shown in Fig. 6.

Each of the four plots of Fig. 6 has the representation of the vapour pressure for five of the compounds used in the parameter estimation. The presence of very different molecules in each plot is due to the proximity of the vapour pressure for similar compounds, making it more difficult to appreciate the results shown. The experimental data used for these plots is referred in 2.1.5. Parameter estimation. The vapour pressure, y axis, is in a logarithmic scale.
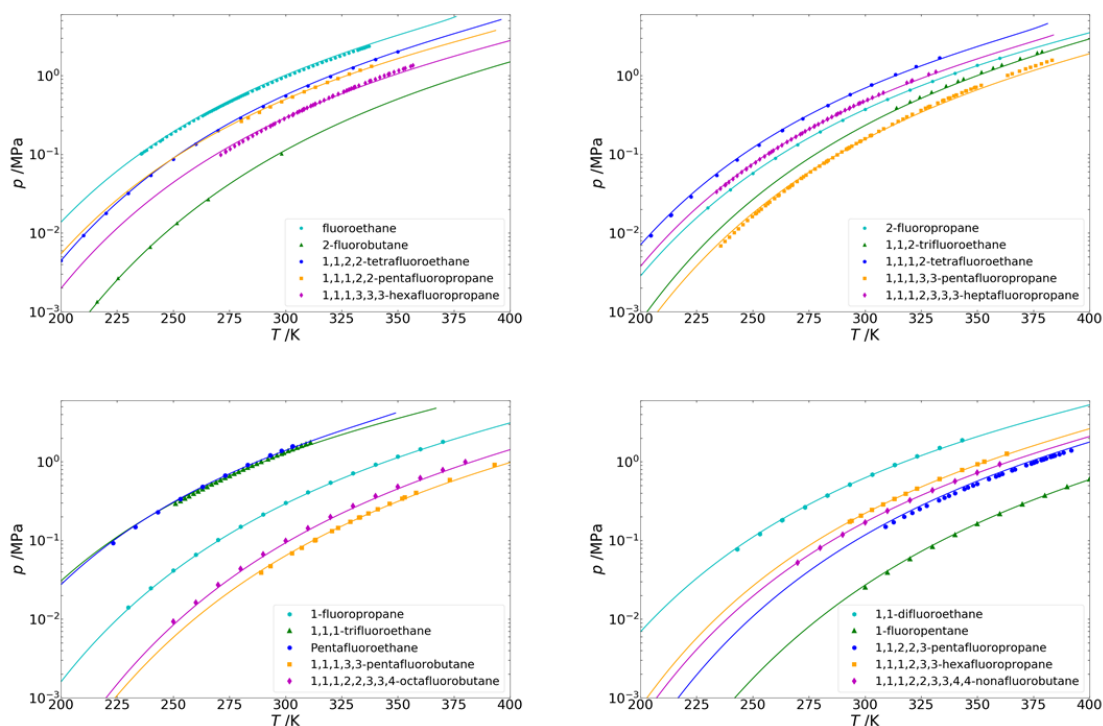
Fig. 6. Vapour pressure analysis of the compounds studied in this section. Curves: calculated vapour pressures. Points: experimental vapour pressures. x axis in logarithmic scale. Experimental data collected in Table 4.

The model description of the vapour pressure fits the experimental data of each compound, meaning that with the estimation of parameters made by fitting both vapour pressures and saturated liquid densities can represent the behaviour of the molecules studied for the vapour pressure.

Additionally, a comparison between the calculated vapour pressure points and the experimental points is shown in the parity plot of the vapour pressure (Fig. 5). The inset plots are an augmented representation of the main parity plot. The bottom right plot represents the low-pressure region between 0 and 0.5 MPa and the upper left one represents the intermediate range, between 0.5 and 1.5 MPa. The dashed lines mark out the area of ±5% deviation from the central or non-deviation line. The points correspond to the range from the triple point and $0.9 \cdot T_{cr}$, for all the compounds employed in this stage.
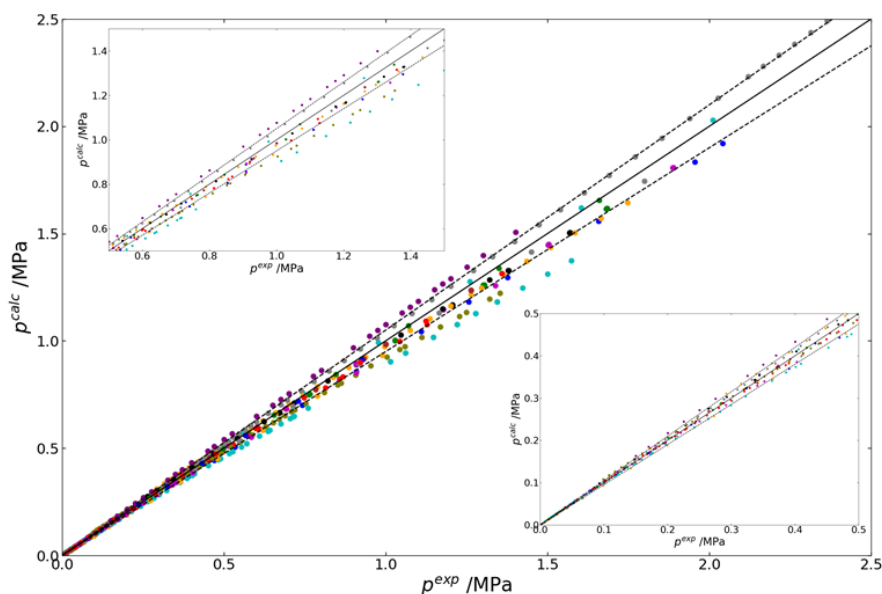
Fig. 7. Parity plot of the vapour pressure: comparison between calculated and experimental vapour pressure. Each colour represents one molecule. The continuous line corresponds to the equality relationship and the dashed lines delimit the ±5% deviation area.

The results of the parity plot allow us to determine that the proposed approach gives an estimation of the vapour pressure mainly inside the ±5% average deviation for all the points considered in the employed range. Furthermore, the estimation does not show bigger deviation at low pressures or at high ones, meaning an appropriate approach using the proposed parameters.

<u>Saturated liquid density</u>

The other property, along with the vapour pressure, used in the parameter optimisation is the saturated liquid density. As was done for the vapour pressure, the results of the saturated density, for the liquid phase, are plotted in Fig. 8. For this property, the y axis represents the temperature in Kelvin, and the x axis the density, in kg·m^{-3}.

For all the compounds implied in the parameter estimation, the saturated liquid densities are represented, gathering this property for five compounds with different ranges of the saturated density in the same plot, to reduce the number of plots. These plots are collected in Fig. 8.
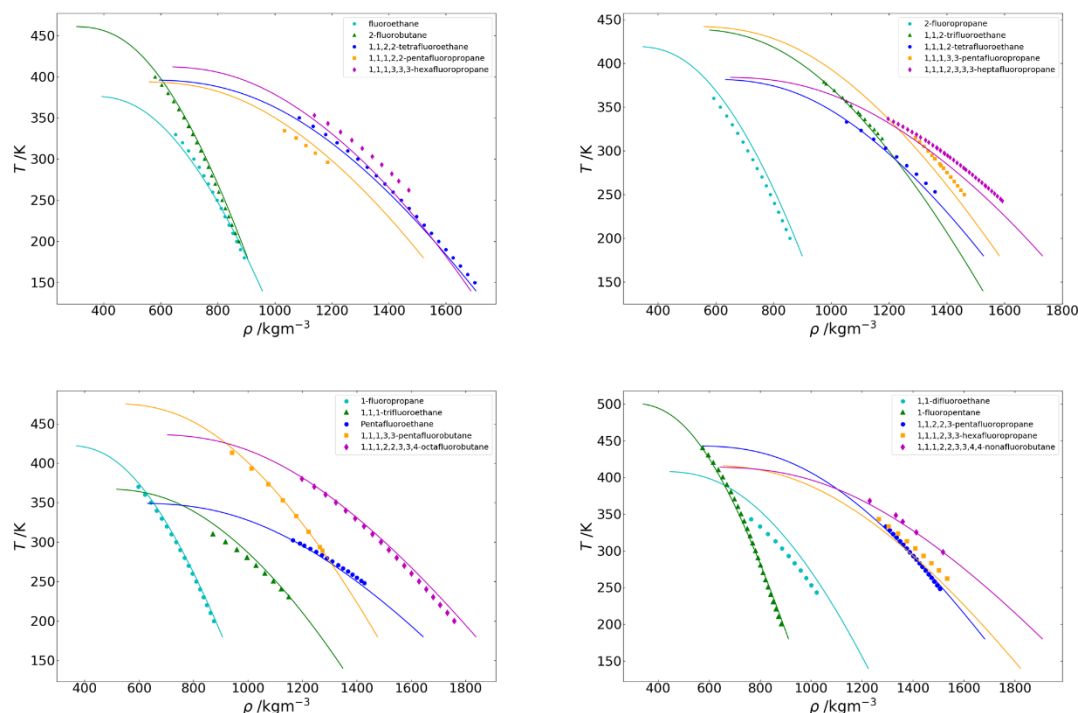
Fig. 8. Saturated liquid density analysis of the compounds studied in this section. Curves: calculated saturated liquid densities. Points: experimental saturated liquid densities. Experimental data collected in Table 4.

In the Fig. 9, the parity plot for the calculated and experimental saturated liquid density is represented. The central line corresponds to the parity line, in which the calculated value equals the experimental value, at the same conditions and for the same compound, whereas the dashed lines delimit the ±5% deviation area. The small plots inside the figure are the augmented parity plots for the low-density region (right plot) and for the intermediate region (upper plot).
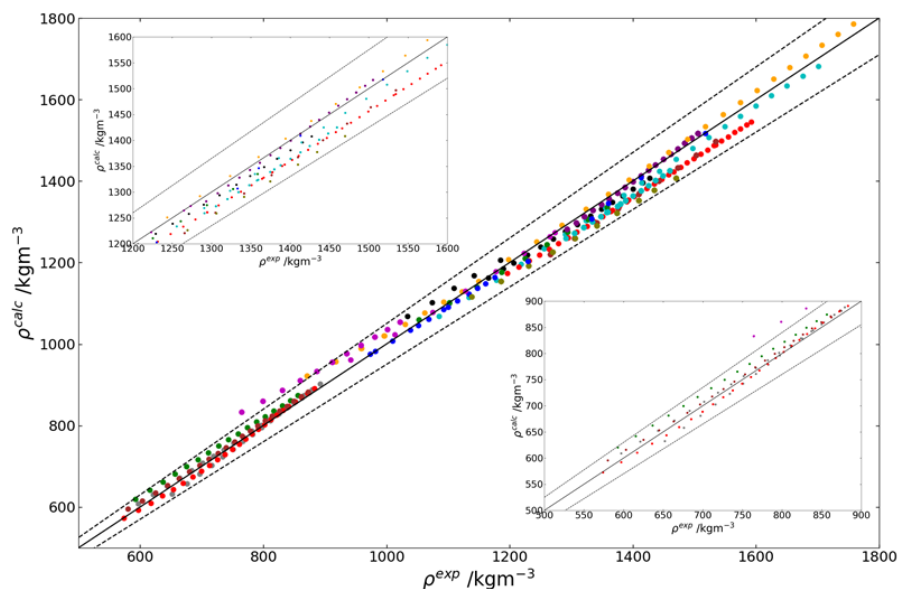

Fig. 9. Parity plot of the saturated liquid density: comparison between calculated and experimental saturated liquid density. Each colour represents one molecule. The continuous line corresponds to the equality relationship and the dashed lines delimit the ±5% deviation area.

According to the comparison between experimental and calculated values for the saturated density, the wide majority of the points fall into the ±5% deviation area. Furthermore, there is no evidence of higher average deviations at either high or low values of the density.

Finally, both properties used for the parameter estimation are analysed calculating the deviation between experimental data and the data calculated with the model proposed at the same conditions for each compound. The Absolute Deviation, AD, represents the mean deviation from experimental data and calculated data, in absolute terms, whereas the Average Absolute Deviation, AAD, is the absolute deviation divided by the experimental value, expressed as a percentage.

$$AD = \frac{1}{N} \sum_{i}^{N} |R_i^{calc} - R_i^{exp}| \qquad [37]$$

$$AAD = \frac{1}{N} \sum_{i}^{N} \frac{|R_i^{calc} - R_i^{exp}|}{|R_i^{exp}|} \cdot 100 \qquad [38]$$

Both deviations for the vapour pressure and the saturated liquid density are collected in Table 8 for all the compounds with experimental data available, considering all the points included in the range between

Table 8. Deviations from experimental data using the proposed parameters. AD: absolute deviation. AAD: average absolute deviation.

Name	Molecular Formula	AD		AAD %	
		p_{vap}/MPa	$\rho_{liq,sat}$/kg·m^{-3}	p_{vap}	$\rho_{liq,sat}$
Pentafluoroethane	C_2HF_5	0.02	12.43	2.50	0.93
1,1,2,2-tetrafluoroethane	$C_2H_2F_4$	0.01	17.32	1.96	1.25
1,1,1,2-tetrafluoroethane	$C_2H_2F_4$	0.01	12.64	3.34	1.00
1,1,2-trifluoroethane	$C_2H_3F_3$	0.06	6.28	5.33	0.57
1,1,1-trifluoroethane	$C_2H_3F_3$	0.03	24.59	3.13	2.61
1,1-difluoroethane	$C_2H_4F_2$	0.02	43.90	2.34	4.95
Fluoroethane	C_2H_5F	0.10	8.98	4.73	1.23
1,1,1,2,3,3,3-heptafluoropropane	C_3HF_7	0.01	37.55	1.61	2.65
1,1,1,2,3,3-hexafluoropropane	$C_3H_2F_6$	0.01	40.66	0.85	2.91
1,1,1,3,3,3-hexafluoropropane	$C_3H_2F_6$	0.03	46.19	4.50	3.44
1,1,2,2,3-pentafluoropropane	$C_3H_3F_5$	0.05	6.38	7.77	0.45
1,1,1,2,2-pentafluoropropane	$C_3H_3F_5$	0.01	25.69	1.85	2.40
1,1,1,3,3-pentafluoropropane	$C_3H_3F_5$	0.03	34.43	6.09	2.50
2-Fluoropropane	C_3H_7F	0.00	21.35	0.34	3.03
1,1,1,2,2,3,3,4,4-nonafluorobutane	C_4HF_9	0.00	15.49	0.69	1.22
1,1,1,2,2,3,3,4-octafluorobutane	$C_4H_2F_8$	0.02	15.61	5.90	1.01
1,1,1,3,3-pentafluorobutane	$C_4H_5F_5$	0.01	4.00	2.98	0.40
1-fluoropropane	$C_5H_{11}F$	0.01	6.31	2.63	0.87
1-fluoropentane	C_3H_7F	0.01	6.19	2.52	0.84
2-fluorobutane	C_4H_9F	0.00	8.43	1.67	1.16

Only four AAD calculated are higher than 5% for the vapour pressure, with an overall AAD of 3.14%, so it can be considered that the parameters proposed represent properly the vapour pressure of the refrigerants proposed. The same can be assumed for the saturated liquid density, with only three compounds with an AAD over 3%, and an overall AAD of 1.77%.

According to the results shown, both the deviations and the figures, the models proposed for the groups involved are adequate to obtain an approach of the pure VLE, as the vapour pressure and the saturated liquid density, for the temperature range from the triple point to a temperature of 90%·T_{cr}.

2.2.2. Properties prediction

Once all the parameters needed are optimised to capture the experimental VLE, other properties of interest are analysed. Following the main objective of the current work, the optimisation of ORC, thermodynamic properties are estimated and compared with experimental data from bibliography. Regarding the thermodynamic properties, in the current work we focus the efforts on temperature—entropy (*T-s* diagrams) diagrams and pressure—enthalpy (*p-h* diagrams) ones. Other thermodynamic properties studied are the isobaric heat capacity, c_p, the speed of sound, u_s, the isobaric coefficient of expansion, α_p, the isothermal compressibility, β_T, and the Joule-Thomson coefficient, μ_{JT}.

In addition to these properties, the binary VLE is studied to know the extent to which the proposed parameters are useful and can be used. As a working fluid for an ORC, a blend of organic molecules can be used, leading in some cases to promising results.

Thermodynamic properties

Finally, entropy and enthalpy are analysed for six compounds. The estimated properties are compared with the experimental data from NIST[32]. Both thermodynamic properties are crucial to simulate cycles to obtain a power output, such as ORCs. Enthalpies are used to estimate the power and energy exchanged in the cycle, and entropies are useful for the isentropic efficiency of both the pump and the expander of the cycle.

The specific entropy is analysed along with the temperature, by plotting the *T-s* diagram estimated with the group contribution approach and the experimental *T-s* diagram. To analyse the accuracy of the studied method, six fluorinated hydrocarbons are analysed, plotting the results in Fig. 10.
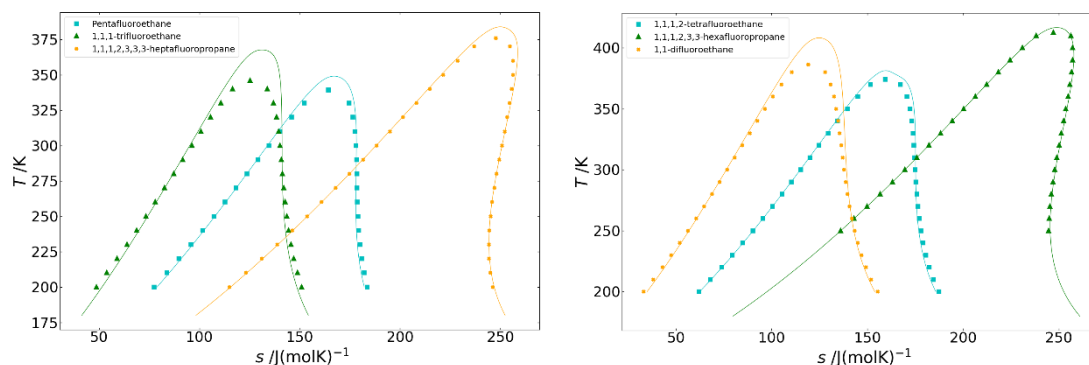

Fig. 10. Temperature-entropy (T-s) diagrams. s: specific entropy, J·(mol·K)⁻¹. T: temperature, K. Curves: calculated entropies with the proposed model. Points: experimental entropies. Reference states: s = 1 J·(g·K)⁻¹ at 0°C.

From the displayed diagrams, it can be concluded that the bigger deviations on the estimation of the entropy, for the studied functional groups, take place near the critical point, at the highest temperature of the VLE. This deviation can be explained as a cumulative error, as the proposed method fails to fit the experimental data, with the same parameters, in the critical region and the rest of VLE. However, the entropy estimation, represented in the diagrams with the continuous line, reproduce adequately the entropy in both the vapour and liquid phase.

In addition to the plots, the deviations from experimental data are collected in Table 9. The absolute deviation [37] and the average absolute deviation [38] are split for the vapour and the liquid phase, and the overall deviations are calculated too. Both deviations are analysed for the entire range of temperatures, from 200K to p_{cr} of each compound.

Table 9. Entropy deviations between experimental and calculated data. AD: absolute deviation. AAD: average absolute deviation.

Compound	Vapour		Liquid		AD /J·(mol·K)$^{-1}$	AAD %
	AD /J·(mol·K)$^{-1}$	AAD %	AD /J·(mol·K)$^{-1}$	AAD %		
Pentafluoroethane	1.7044	0.99	1.3640	1.07	1.5342	1.03
1,1,1-trifluoroethane	2.8041	2.08	2.2075	2.54	2.5058	2.31
1,1,1,2,3,3,3-heptafluoropropane	1.1268	0.45	0.9825	0.46	1.0546	0.46
1,1,1,2-tetrafluoroethane	1.7445	1.02	0.9068	0.68	1.3257	0.85
1,1,1,2,3,3-hexafluoropropane	0.9075	0.36	0.4229	0.18	0.6652	0.27
1,1-difluoroethane	2.8182	2.17	1.5573	1.97	2.1878	2.07

As reflected in the deviations calculated and the *T-s* diagrams, the proposed parameters for the selected functional groups within the SAFT-γ Mie method can reproduce with a deviation under 3% the entropy of the six molecules selected. The maximum deviation calculated corresponds to the 1,1,1-trifluoroethane, the compound with a higher deviation in the vapour pressure, according to Table 8. The lowest deviation, corresponding to the 1,1,1,2,3,3-hexafluoropropane, reflects the low deviation in the vapour pressure for this molecule.

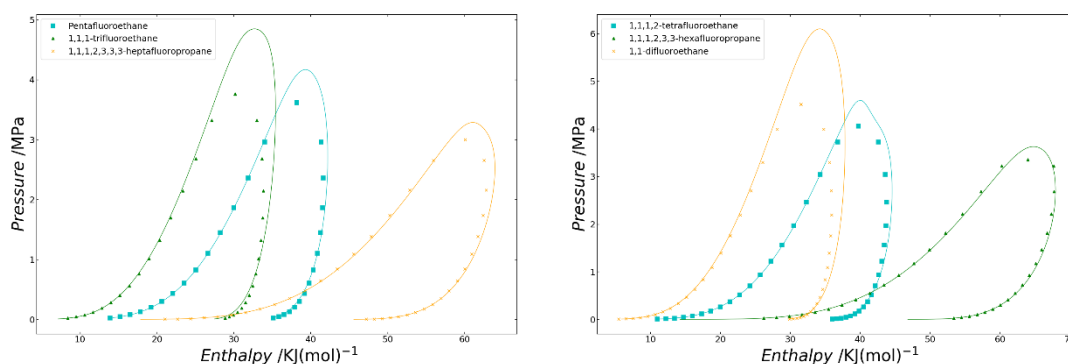The enthalpy is represented with the pressure in the *p-h* diagram (Fig. 11).

Fig. 11. Pressure-enthalpy (p-h) diagrams. h: specific enthalpy, kJ·(mol)$^{-1}$. *p: pressure,* MPa. *Curves: calculated enthalpies with the proposed model. Points: experimental enthalpies. Reference states: h =* 200 kJ·kg^{-1} at 0°C.

As for the entropy, the proposed approach predicts the enthalpy properly from low temperatures near the triple point, until temperatures near the critical point. The higher deviations are found to occur in the critical region, due to the lack of accuracy prediction the VLE at this temperatures and pressures for the studied compounds.

The calculated deviations ([37][38]) for the enthalpy of the compounds represented in the displayed diagrams are collected in Table 10. The AD and AAD are calculated for the saturated vapour phase enthalpy, the saturated liquid phase enthalpy and the overall for each compound.

Table 10. Enthalpy deviations between experimental and calculated data. AD: absolute deviation. AAD: average absolute deviation.

Compound	Vapour		Liquid		AD	AAD
	AD /kJ·(mol)$^{-1}$	AAD %	AD /kJ·(mol)$^{-1}$	AAD %	/kJ·(mol)$^{-1}$	%
Pentafluoroethane	0.5325	1.39	0.6810	2.09	0.6067	1.74
1,1,1-trifluoroethane	0.7299	2.34	1.3580	5.48	1.0440	3.91
1,1,1,2,3,3,3-heptafluoropropane	0.4288	0.71	0.7429	1.46	0.5859	1.09
1,1,1,2-tetrafluoroethane	2.0457	5.05	0.3098	1.55	1.1778	3.30
1,1,1,2,3,3-hexafluoropropane	0.4169	0.65	0.7100	1.23	0.5635	0.94
1,1-difluoroethane	1.0191	3.02	0.3084	1.58	0.6638	2.30

The tendency shown in the deviations for the enthalpy is the same as for the entropy, obtaining a lower deviation for those compounds with a better prediction of the VLE. It can be assumed that the proposed approach is a valid one to estimate the enthalpy, as reflected in the deviations table and the *p-h* diagrams. All the calculated deviations are below 4% average absolute deviation.

Finally, both main thermodynamic properties, enthalpy and entropy, can be estimated adequately with the SAFT-γ Mie equation of state, using the parameter estimated by adjusting the vapour pressure and the saturated liquid density. The estimation of these properties allow the use of this accurate group contribution approach to model ORCs, as a further step of the current work.

Other thermodynamic properties

The calorific properties involved in this validation step are defined below. The isobaric heat capacity,

$$c_p = \left(\frac{\partial h}{\partial T}\right)_p \qquad [39]$$

the Joule-Thomson coefficient,

$$\mu_{\mathrm{JT}} = \left(\frac{\partial T}{\partial p}\right)_h = -\frac{\left(\frac{\partial h}{\partial p}\right)_T}{\left(\frac{\partial h}{\partial T}\right)_p} = -\frac{V - T\left(\frac{\partial V}{\partial T}\right)_p}{c_p} \qquad [40]$$

the speed of sound,

$$u_s^2 = \left(\frac{\partial p}{\partial \rho}\right)_s \qquad [41]$$

the isobaric coefficient of expansion,

$$\alpha_p = \frac{1}{V} \cdot \left(\frac{\partial V}{\partial T}\right)_p \qquad [42]$$

and the isothermal compressibility,

$$\beta_T = -\frac{1}{V} \cdot \left(\frac{\partial V}{\partial p}\right)_T \qquad\qquad [43]$$

These properties are estimated for three fluorinated hydrocarbons, pentafluoroethane, 1,1,1,2-tetrafluoroethane and 1,1,1,2,3,3,3-heptafluoroethane, and compared with pseudo experimental data available from NIST/TRC[32]. These properties depend on the temperature and pressure at the same time, so the plots represent the model, cope with the experimental data, at fixed values of the pressure, reflecting the temperature effect at each temperature.

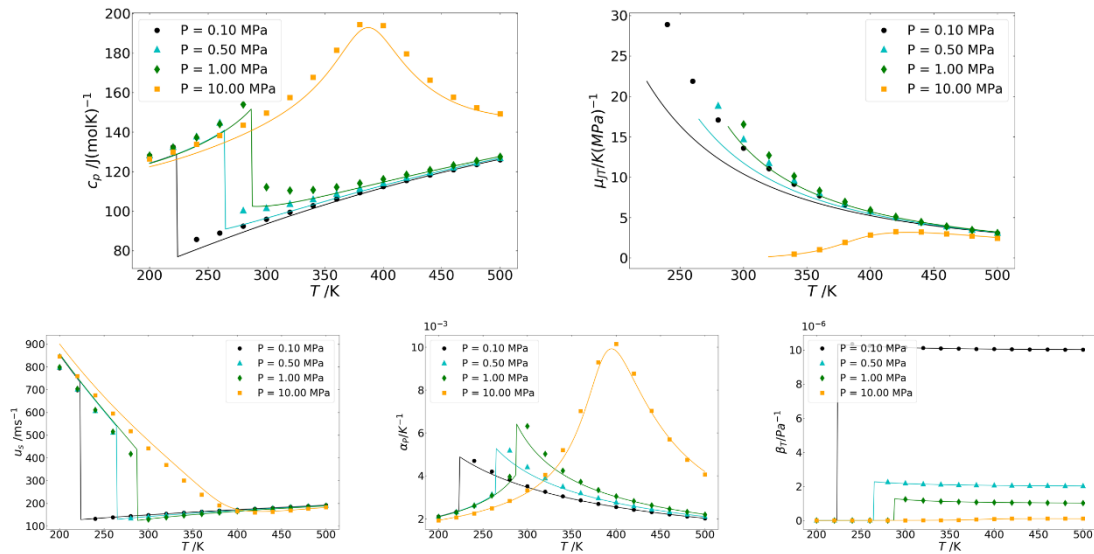First of all, pentafluoroethane (R-125) calorific performance is analysed and plotted in Fig. 12.

Fig. 12. Calorific properties of pentafluoroethane. Upper row: Left: Isobaric heat capacity. Right: Joule-Thomson coefficient. Lower row: From left to right: Speed of sound, isobaric coefficient of expansion and isothermal compressibility.

As reflected in the plots, the proposed method is able to estimate the calorific properties selected with a good accuracy, except for the Joule-Thomson coefficient at low temperatures, where a higher deviation is obtained. The AAD calculated for the isobaric heat capacity, c_p, is 2.75%, whereas the AAD for the Joule-Thomson coefficient, μ_{JT}, is 9.01%.

The second compound analysed, the 1,1,1,2-tetrafluoroethane (R-134a), is represented in Fig. 13.
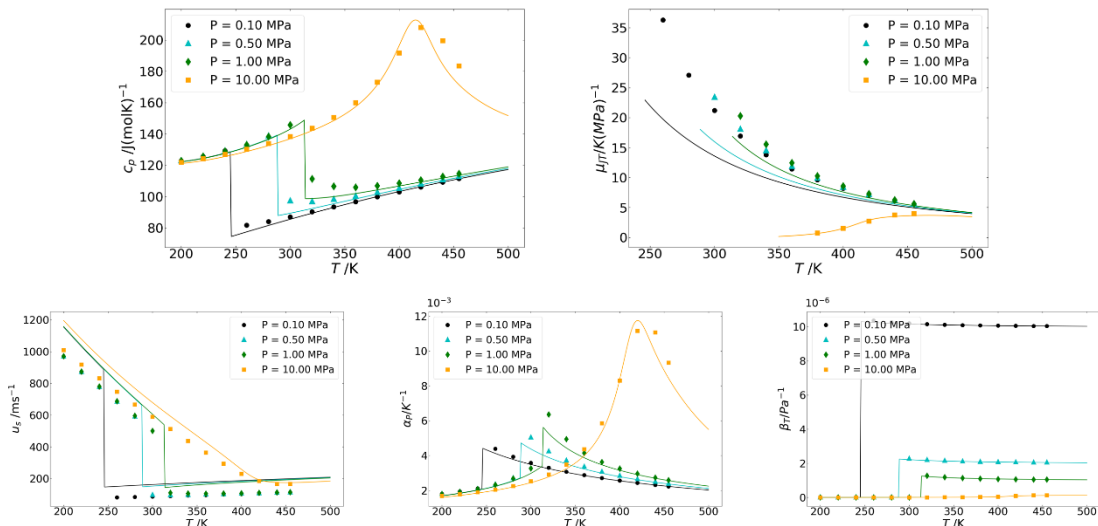
Fig. 13. Calorific properties of 1,1,1,2-tetrafluoroethane. Upper row: Left: Isobaric heat capacity. Right: Joule-Thomson coefficient. Lower row: From left to right: Speed of sound, isobaric coefficient of expansion and isothermal compressibility.

The performance of the proposed approach on the calorific properties of R-134a show a bigger deviation, reaching an AAD of 17.52% for the Joule-Thomson coefficient, and an AAD of 2.06% for the isobaric heat capacity. Furthermore, the plots of the remaining properties studied have bigger deviations, as shown for the speed of sound, compared with pentafluoroethane predictions.

Calorific properties of the last compound analysed, the 1,1,1,2,3,3,3-heptafluoropropane (R-227ea), are plotted in Fig. 14.
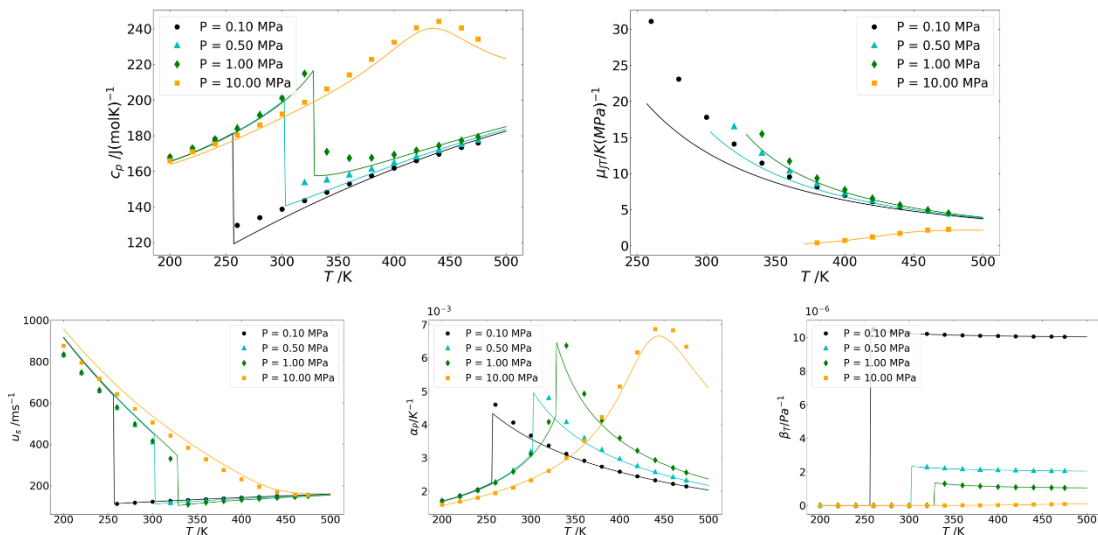

Fig. 14. Calorific properties of 1,1,1,2,3,3,3-heptafluoropropane. Upper row: Left: Isobaric heat capacity. Right: Joule-Thomson coefficient. Lower row: From left to right: Speed of sound, isobaric coefficient of expansion and isothermal compressibility.

The AAD calculated for the c_p is 1.74%, whereas the AAD for μ_{JT} is 9.75%. The predicted properties have good agreement with experimental data, performing better at low temperatures, near the triple point, and at temperatures over 400K. Bigger deviations are found

to take place near the changing phase region. This deviation can be explained as a cumulative error from the VLE estimation.

The deviations between experimental and model data are calculated for both, the isobaric heat capacity and the Joule-Thomson coefficient. The AD and the AAD are collected in Table 11.

Table 11. Isobaric heat capacity , c_p, and Joule-Thomson coefficient, μ_{JT}, deviations

Compound	c_p		μ_{JT}	
	AD /J·(mol·K)$^{-1}$	AAD%	AD /K·(MPa)$^{-1}$	AAD %
Pentafluoroethane	4.3582	2.76	1.0044	9.01
1,1,1,2-tetrafluoroethane	3.2682	2.06	2.5025	17.52
1,1,1,2,3,3,3-heptafluoropropane	3.1612	1.74	1.2141	9.75

The description of the isobaric heat capacity and the Joule-Thomson Coefficient provided by the model studied in the current work provides an adequate description of the experimental data. Furthermore, the isobaric heat capacity, c_p, has a low AAD for the three compounds analysed at this step, in all the cases under 3%. This property of the working fluid is widely used for process modelling. In the case of the Joule-Thomson coefficient, μ_{JT}, bigger deviations are obtained when comparing the results using the proposed model with the experimental data collected. One of the main reasons of this deviation with respect to the experimental data is the ideal-heat-capacity contribution, estimated in the proposed method with the Joback-Reid correlation[12]. This correlation does not perform well for halogenated compounds. To reduce this error, that is found to be bigger for fluorinated compounds, a new correlation is being developed[47].

<u>Binary VLE</u>

The interaction and behaviour of the mixtures of fluorinated hydrocarbons with themselves, alkanes and perfluoroalkanes is analysed with the proposed parameters for the functional groups within the SAFT-γ Mie by means of the binary vapour-liquid equilibrium (VLE).

Binary VLE is represented in the current work in pressure—composition (*pxy*) diagrams, due to the availability of experimental data. In this type of diagram, equilibrium pressure is represented as a function of the mixture composition at constant temperature. The upper curve corresponds to the bubble curve, in which the bubble pressure is represented at each composition. The region over this curve corresponds to the liquid phase, and the region between the bubble and dew curves, the coexistence of a vapour and a liquid phase. The area below the dew curve corresponds to the vapour phase.

In each figure, two binary VLE plots are represented. Each curve represents the isothermal VLE, at the temperature shown in each legend. The x axis represents the concentration, in mole fraction, of the second compound of the mixture represented in the plot.

Fig. 15 represents, on the left side, the VLE of the mixture hexafluoroethane / 1,1,1,2-tetrafluoroethane, at four different temperatures. The right plot corresponds to the mixture of pentafluoroehtane / 1,1,1,2,3,3,3-heptafluoroethane.
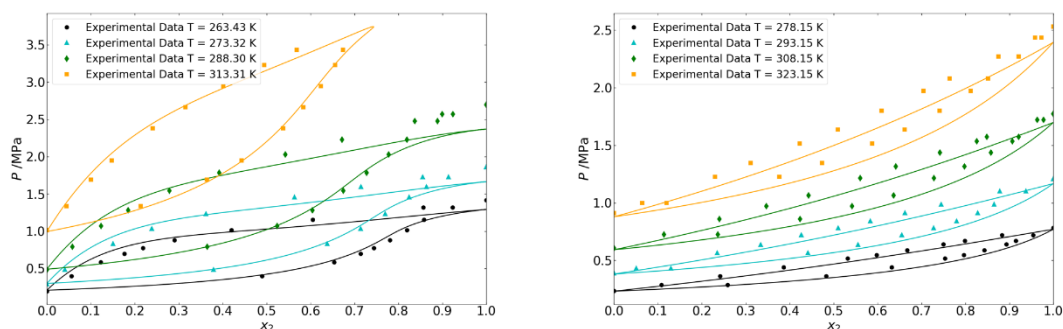
Fig. 15. Left: hexafluoroethane/1,1,1,2-tetrafluoroethane. Right: pentafluoroethane/1,1,1,2,3,3,3-heptafluoropropane.

Both phase diagrams are adequately predicted with the proposed parameters and equation of state. However, in both plots, the deviation increases at high values of the composition of the second molecule, near the pure regions ($x = 1$). To explain the deviation near the pure compound VLE, it is found that the temperature considered is near the critical point of the second compound, making the deviation in the pure vapour pressure bigger. As explained before, the experimental data selected for the parameter optimisation was taken until 90% of T_{cr} because of analytical EoS are not able to capture the critical and subcritical regions with the same parameters, leading to higher deviation near the critical point for the pure compound.
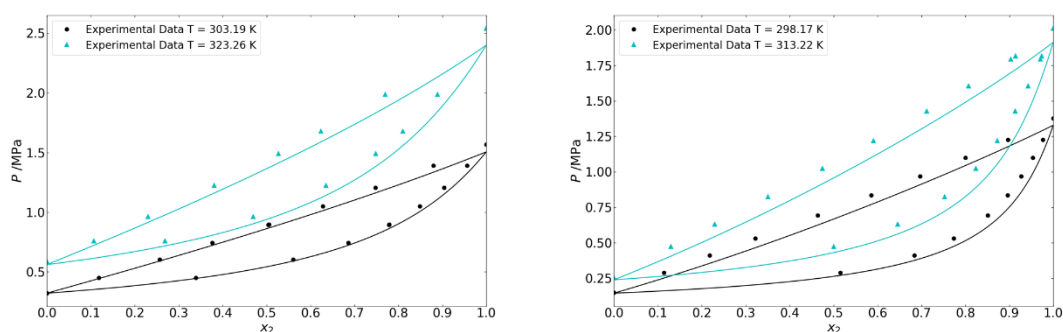

Fig. 16. Left: pentafluoroethane/1,1,1,3,3,3-hexafluoropropane. Right: pentafluoroethane/1,1,1,3,3-pentafluoropropane.

The right plot of Fig. 16 corresponds to the binary VLE, at two constant temperatures, of pentafluoroethane/1,1,1,3,3,3,3-hexafluoropropane. The *pxy* diagram reflects a good fitting between experimental and predicted data, resulting in an AAD of 3.94%. The right plot, corresponding to the blend of pentafluoroethane/1,1,1,3,3-pentafluoropropane, also reflects the agreement of experimental and model data, with an AAD of 8.52%.
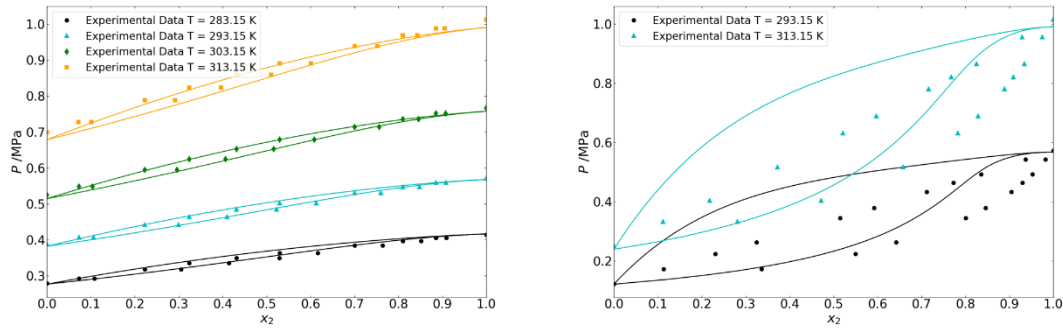
Fig. 17. Left: 1,1,1,2-tetrafluoroethane/1,1,1,2,3,3,3-heptafluoropropane. Right: 1,1,1,2-tetrafluoroethane/1,1,1,3,3-pentafluoropropane.

In Fig. 17, the mixture of 1,1,1,2-tetrafluroethane/1,1,1,2,3,3,3-heptafluoropropane (left plot) and with 1,1,1,3,3-pentafluoropropane, are collected. The first mixture was adequately predicted with the proposed method, with and AAD of 1.33%, whereas the plot on the right reflects a disagreement between experimental and predicted points, overpredicting the equilibria pressures. However, the model is able to predict the shape of the VLE, although the values of the pressure do not match, predicting the VLE in a qualitative way, but not in a quantitative way.

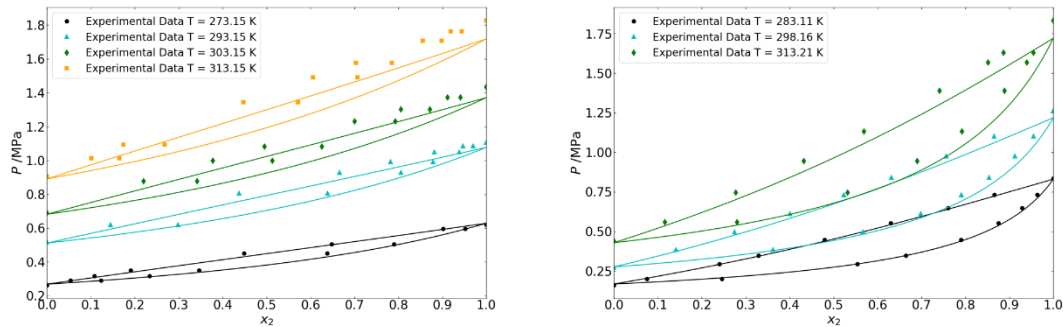*Fig. 18. Left: 1,1,1-trifluoroethane/1,1-difluoroethane. Right: 1,1,1-trifluoroethane/1,1,1,3,3,3-hexafluoropropane.*

Both binary VLEs plotted in Fig. 18 reflect a good agreement of the model with the experimental points, with an AAD of 4.14% for the mixture on the and 3.74% for the right one.

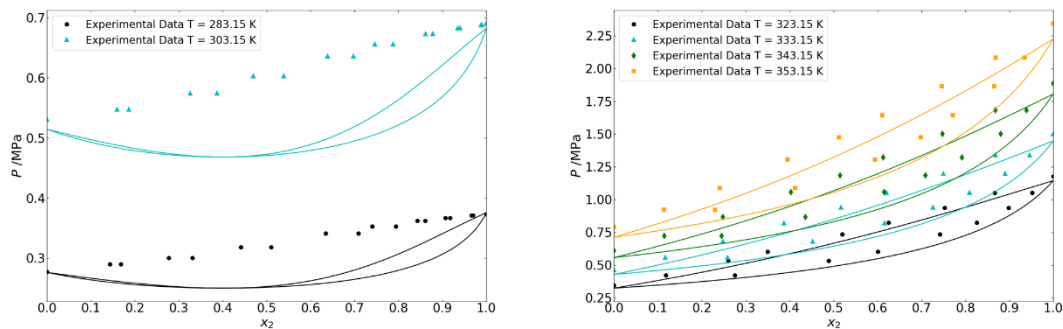*Fig. 19. Left: 1,1-difluoroethane/1,1,1,2,3,3,3-heptafluoropropane. Right: 1,1-difluoroethane/1,1,1,3,3-pentafluoropropane.*

37

The left plot of Fig. 19, the mixture of 1,1-difluroethane/1,1,1,2,3,3,3-heptafluoropropane, results in an inadequate prediction of the binary VLE of both compounds. In this case, the model also fails to predict the shape of the *pxy* diagram, underpredicting the pressure for a given composition. The proposed parameters are calculated from pure experimental data, leading to parameters in which the interaction between different groups is forced, as they are part of the same molecule. However, the interaction of these groups when they are present in different molecules is not the same, like happens in these mixtures, where the VLE prediction leads to non-idealities, whereas the experimental data reflects the real mixture behaviour. This effect is not captured with the proposed method and that would imply the use of secondary-order group effects. The right plot corresponds to the mixture of 1,1-difluoroethane /1,1,1,3,3-pentafluoropropane. The model predicts the binary VLE with an AAD of 7.55%.

Additionally, the AAD of the equilibria pressures calculated referred to the experimental are displayed in Table 12 for the blends plotted previously.

Table 12. AAD calculated for the binary mixtures. AAD: average absolute deviation.

Compound 1	Compound 2	AAD %
Hexafluoroethane	1,1,1,2-tetrafluoroethane	6.24
pentafluoroethane	1,1,1,2,3,3,3-heptafluoropropane	5.70
pentafluoroethane	1,1,1,3,3,3-hexafluoropropane	3.94
pentafluoroethane	1,1,1,3,3-pentafluoropropane	8.52
1,1,1,2-tetrafluoroethane	1,1,1,2,3,3,3-heptafluoropropane	1.33
1,1,1,2-tetrafluoroethane	1,1,1,3,3-pentafluoropropane	26.29
1,1,1-trifluoroethane	1,1-difluoroethane	4.14
1,1,1-trifluoroethane	1,1,1,3,3,3-hexafluoropropane	3.74
1,1-difluoroethane	1,1,1,2,3,3,3-heptafluoropropane	11.55
1,1-difluoroethane	1,1,1,3,3-pentafluoropropane	7.55

As reflected in both the plots and the AADs, the proposed method can estimate the binary interaction adequately when compounds with a similar number of fluorine atoms, with a similar arrangement, are involved, but fail to predict the VLE otherwise.

The proposed parameters are unable to capture the behaviour of some VLE, due to local polarisation effects on the molecules as a result of the presence of high electronegative fluorine atoms, predicting with the optimised parameters non-idealities in the mixtures, whereas experimental data show a different VLE.

This failure in the capture of binary VLE leads to the need of second-order interaction parameters to capture the interaction between these groups. The unlike energy parameter is estimated using pure VLE, so the estimated parameter is useful when the interaction occurs inside the same molecule. Nevertheless, when using these parameters in binary mixtures, with

different groups involved, an inadequate prediction of the VLE is obtained. The behaviour of a functional group is not the same when the adjacent group parameters are not the same. To solve this failure in the prediction, secondary-order group parameters can be estimated, removing big errors when estimated the binary behaviour of every mixture of alkanes, perfluoroalkanes and fluorinated alkanes.

3. Organic Rankine Cycle analysis

3.1. Methods/Theory

3.1.1. Thermophysical properties for ORC modelling

In addition to the thermodynamic properties calculated with the SAFT-γ Mie equation of state, transport properties are necessary to estimate the sizing of the ORC equipment and then estimate the specific investment cost, SIC[20,24]. The main properties to estimate are the surface tension, γ, the liquid and vapour viscosity, μ_L and μ_V, and finally the liquid and vapour thermal conductivity, k_L and k_V. Furthermore, a detailed description of the methods employed in the current work to obtain the critical point and the normal boiling point are appended.

Following the approach to estimate the thermophysical properties of the working fluid, a similar method for each property is desired. As the main objective is to design a CAMD-ORC, in which the working fluid is designed as the addition of several functional groups, a group contribution approach for each remaining property is desired. Below, a full description of the path followed to estimate those properties is explained.

In the group contribution approaches, the fluid is described by the functional groups present in the molecule, as well as the number of each of those groups. The groups studied in the current work are: CH_3, CH_2, CH_2F, CHF, CHF_2, CF_3, CF_2. Among all the group contribution methods to obtain the following properties, the ideal method should not include a second order contribution, because that will lead to a greater complexity, which is undesirable. Also, specific correction factors or modifications are not desired in the current work.

Normal boiling point

The normal boiling temperature is a property used later for the correlations of the transport properties. Two methods are selected to estimate this property of a fluid.

First of all, the Joback-Reid normal-boiling-point correlation[12], to obtain this temperature is described in equation [44].

$$T_B = 198.2 + \sum_i n_i \cdot C_i^{T_B}$$

[44]

The parameter $C_i^{T_B}$ refers to the coefficient from the reference for the normal boiling point for each group i, n_i to the number of groups of type i in the fluid and T_B is the normal boiling point in Kelvin. In Table 13 all the coefficients for the functional groups of interest are collected, together with the rest of coefficient for the critical properties.

On the other hand, the SAFT-γ Mie approach can also be used to obtain the normal boiling point. The chemical potential, μ_i, of species i is calculated as a partial derivate of the free energy

$$\frac{\mu_i}{kT} = \left(\frac{\partial A/kT}{\partial N_i}\right)_{T,V,N_{j\neq i}}$$

[45]

where N_i is the number of chain molecules of species i. To obtain the equilibrium for two or more phases, pressures, temperatures and chemical potentials of each component need to be equal in each phase. The normal boiling point is calculated as follows

$$\mu_i^L(T,p) = \mu_i^V(T,p)$$

[46]

$$p = 101325 \ \text{Pa} \ \rightarrow \ T_B = T$$

[47]

where the VLE is calculated [46] until the atmospheric pressure is reached [47], and the normal boiling point T_B is obtained.

Critical point

The critical point, described by the critical temperature, T_{cr}, the critical pressure, p_{cr}, and the critical volume, v_{cr}, allows the estimation of some transport properties. Among the wide variety of methods to estimate the critical point, the main two group-contribution methods are highlighted.

First of all, the group contribution equation of state, SAFT-γ Mie, previously described to estimate the thermodynamic properties of the working fluid, can be used to obtain the properties of the critical point of a molecule. The method proposed in this section to obtain the critical point with this approach consists of varying the temperature, T, calculating the phase equilibrium [48] and then iterating until condition [49] is satisfied.

$$\mu_i^L(T,p) = \mu_i^V(T,p) \tag{48}$$

$$\frac{V^V(T,p)}{V^L(T,p)} \leq 1 + \varepsilon \tag{49}$$

The variable ε could take any value, in this case 0.2 is used. When the condition is satisfied, the critical point is reached to within the prescribed tolerance and then $T_{cr} = T$, $p_{cr} = p$ and $V_{cr} = (V^V + V^L)/2$.

The other method to obtain the critical point is a correlation[12] described in equations [2-4]. Each equation describes the correlation for the three properties of the critical point. The advantage of this group is the low computational cost in contrast to the other method. All the coefficients used below are collected in Table 13.

$$T_{cr} = \frac{T_B}{0.584 + 0.965 \cdot \sum_i n_i \cdot C_i^{T_{cr}} - \left(\sum_i n_i \cdot C_i^{T_{cr}}\right)^2} \tag{50}$$

where T_{cr} is the critical temperature in Kelvin, T_B the normal boiling point in Kelvin, and $C_i^{T_{cr}}$ the coefficient of each functional group for the critical temperature.

$$p_{cr} = \left(0.113 + 0.0032 \cdot \sum_i n_i - \sum_i n_i \cdot C_i^{p_{cr}}\right)^{-2} \tag{51}$$

where p_{cr} is the critical pressure in bar, n_i the number of atoms of the functional group i and $C_i^{p_{cr}}$ the coefficient for the critical pressure of the group i.

$$V_{cr} = 17.5 + \sum_i n_i \cdot C_i^{V_{cr}} \tag{52}$$

where V_{cr} is the critical volume in cm³·mol⁻¹ and $C_i^{V_{cr}}$ the coefficient for the critical volume of the group i. The term n_i in the three equations refers to the number of groups of type i in the fluid studied.

Table 13. Joback-Reid coefficients[12]. $C_i^{T_B}$: normal boiling point coefficient for group i. $C_i^{T_{cr}}$: critical temperature coefficient for group i. $C_i^{p_{cr}}$: critical pressure coefficient for group i . $C_i^{V_{cr}}$: critical volume coefficient for group i . n_i: number of atoms present in group i

Functional group	$C_i^{T_B}$	$C_i^{T_{cr}}$	$C_i^{p_{cr}}$	$C_i^{V_{cr}}$	n_i
CH_3	23.58	0.0141	-0.0012	65	4
CH_2	22.88	0.0189	0.0000	56	3
CF_3	18.16	0.0400	-0.0128	108	4
CF_2	18.19	0.0289	-0.0071	81	3
CH_2F	22.85	0.0300	-0.0057	83	4
CHF	21.71	0.0275	-0.0037	68	3
CHF_2	21.68	0.0386	-0.0094	95	4

Surface tension

The surface tension, σ, is estimated using the Sastri-Rao[48] correlation, shown in equation [53]. This method is not a group contribution one, but it takes into account the critical point and the normal boiling temperature, calculated with the previous correlations.

$$\gamma = K \cdot p_{cr}^x \cdot T_B^y \cdot T_{cr}^z \cdot \left[\frac{1 - T_r}{1 - T_{B,r}}\right]^m \tag{53}$$

where γ is the surface tension of the liquid in mN·m^{-1}, T_B the normal boiling point in Kelvin, T_{cr} the critical temperature in Kelvin, p_{cr} the critical pressure in bar, $T_{B,r} = T_B/T_{cr}$ the reduced boiling temperature and $T_r = T/T_{cr}$ the reduced temperature. The rest of the variables represent the parameters of the correlation and the values employed are collected in Table 14.

Table 14. Coefficients for the surface tension[48]

K	x	y	z	m
0.158	0.5	-1.5	1.85	11/9

Viscosity

To obtain the viscosity, first of all we have to distinguish between the liquid and vapour phase. For each phase, a different correlation is proposed, as the order of magnitude is different.

Liquid viscosity, η_L

In order to calculate the saturated liquid viscosity, the correlation [54] is selected[49].

$$\eta_L = \sum_i n_i \cdot C_i^{\eta_B} \cdot p_{vap}^{-[0.2 + \sum_i C_i^{\eta_n}]} \tag{54}$$

where η_L is the liquid viscosity in mPa·s, p_{vap} the vapour pressure in bar, $C_i^{\eta_B}$ the normal boiling point coefficient, n_i the number of groups of type i in the fluid and $C_i^{\eta_n}$ the exponential coefficient of the viscosity. The value of the coefficients collected in Table 15. The values of the vapour pressure are obtained with the thermodynamic model for the temperature of reference. The summation in the exponential of the vapour pressure, as reflected in the equation, only takes the coefficient once if this group is present in the fluid.

Vapour viscosity, μ_V

For the viscosity of the vapour phase, correlation [55] is employed. This correlation could be used with a dipole moment correction. Nevertheless, due to the need of a group contribution method to obtain the dipole moment, which includes second order contributions, this term is not reflected in the final correlation. The high-pressure correction is also neglected, as the process of interest occurs at low to medium pressures.

$$\eta_V = \frac{M^{0.5} \cdot T}{\sum_i n_i \cdot C_i^{\eta_V} \left(1 + 0.36 \cdot \left(1 + \frac{4}{T_{cr}}\right) \cdot T_r \cdot (T_r - 1)\right)^{\frac{1}{6}} \cdot 100} \tag{55}$$

where η_V is the vapour dynamic viscosity in µPa·s, M is the relative molecular mass of the fluid, T the temperature in K, T_{cr} the critical temperature in K, $T_r = T/T_{cr}$ the reduce temperature and $C_i^{\eta_V}$ the coefficient for the vapour dynamic viscosity for each group, collected in Table 15.

The correlation proposed included a dipole moment correction factor, neglected in the current work due to the difficulty of developing a dipole moment group contribution method without a second-order contribution.

Table 15. Coefficients for viscosity correlations[49,50]. $C_i^{\eta_B}$: normal boiling point liquid viscosity coefficient for group i. $C_i^{\eta_n}$: exponential liquid viscosity coefficient for group i. $C_i^{\eta_V}$: vapour viscosity coefficient for group i.

Functional group	$C_i^{\eta_B}/\mathrm{mPa} \cdot \mathrm{s}$	$C_i^{\eta_n}$	$C_i^{\eta_V}/10^{-8}(\mathrm{Pa} \cdot \mathrm{s})^{-1}$
CH_3	0.105	0.00	0.904
CH_2	0.000	0.00	0.647
CF_3	0.165	0.10	1.185
CF_2	0.050	0.10	0.739
CH_2F	0.185	0.00	1.093
CHF	0.045	0.05	0.713
CHF_2	0.200	0.05	1.159

Thermal conductivity

As for the viscosity, there is a difference in the way to obtain the thermal conductivity of liquid and vapor phases, so both methods are split.

Liquid thermal conductivity, k_L

The liquid thermal conductivity[51] is calculated with eq. [56]. The term m is calculated as reflected in eq. [57]. The original correlation also includes a correction term that is neglected because it is not a group contribution term, it depends on the type of fluid, like alkanes or perfluoralkanes.

$$k_L = \sum_i (n_i \cdot C_i^{k_B}) \cdot a^m \tag{56}$$

$$m = 1 - \left(\frac{1 - T_r}{1 - T_{B,r}}\right)^n \tag{57}$$

where k_L is the liquid thermal conductivity in W·m^{-1}·K^{-1}, a factor which value is 0.16 for all the substances considered, n a factor of 0.2, $T_r = T/T_{cr}$ the reduced temperature, $T_{B,r} = T_B/T_{cr}$ the

reduced boiling temperature, and $C_i^{k_B}$ the coefficient of the group i for the thermal conductivity, that takes the values collected in Table 16.

Table 16. Coefficients for liquid thermal conductivity[51]. $C_i^{k_l}$: liquid thermal conductivity coefficient for group i.

Functional group	$C_i^{k_L}/\mathrm{W} \cdot \mathrm{m}^{-1} \cdot \mathrm{K}^{-1}$
CH_3	0.0545
CH_2	-0.0008
CF_3	0.0474
CF_2	-0.0094
CH_2F	0.0502
CHF	-0.0090
CHF_2	0.0420

<u>Vapour thermal conductivity, k_V</u>

The proposed method for the vapour thermal conductivity[50,52] is not a group contribution, however, it depends on previously calculated properties, as the dynamic viscosity or the heat capacity.

$$k_V = \frac{3.75 \cdot \eta_V \cdot R}{M_m{}'} \cdot \psi \qquad [58]$$

where k_V is the vapour thermal conductivity in $\mathrm{W \cdot m^{-1} \cdot K^{-1}}$, R is the ideal gas constant ($R = 8.314 \, \mathrm{J \cdot mol^{-1} \cdot K^{-1}}$), M' is the molar mass in $\mathrm{kg \cdot mol^{-1}}$ and η_V the vapour dynamic viscosity in Pa·s. Factor ψ is calculated with eq. [59].

$$\psi = 1 - \frac{\alpha(0.215 + 0.28288 \cdot \alpha - 1.061 \cdot \beta + 0.26665 \cdot Z)}{0.6366 + \beta \cdot Z + 1.061 \cdot \alpha \cdot \beta} \qquad [59]$$

where factors α, β and Z are calculated with equations [60],[61] and [62] respectively.

$$\alpha = \frac{c_V}{R} - \frac{3}{2} \qquad [60]$$

$$\beta = 0.7862 - 0.7109 \cdot \omega + 1.3168 \cdot \omega^2 \qquad [61]$$

$$Z = 2 + 10.5 \cdot T_r^2 \qquad [62]$$

where c_V is the isochoric heat capacity in $\mathrm{J \cdot mol^{-1} \cdot K^{-1}}$, ω the acentric factor of the molecule and $T_r = T/T_{cr}$ the reduced temperature.

The acentric factor mentioned above, ω, is a property of the fluid and it does not depend on the temperature or other factors. Its value is obtained with eq. [63], and it is defined at a reduced temperature of 0.7.

$$\omega = -1 - \log_{10} \frac{p_{vap}(T_r = 0.7)}{p_{cr}} \qquad [63]$$

To sum up, in Table 17 all the methods involving the estimation of the transport properties of interest described previously are collected with the corresponding references to the bibliography.

Table 17. Summary of the methods/correlations used for transport properties

Property		Methods	Reference
Normal boiling point		Joback-Reid	[12]
Critical temperature		SAFT-γ Mie / Joback-Reid	[2,12]
Critical pressure		SAFT-γ Mie / Joback-Reid	[2,12]
Critical volume		SAFT-γ Mie / Joback-Reid	[2,12]
Surface tension		Sastri-Rao	[48]
Viscosity	Liquid	Sastri-Rao	[49]
	Vapour	Reichenberg	[53]
Thermal conductivity	Liquid	Sastri-Rao	[51]
	Vapour	Chung	[50,52]

3.1.2. Organic Rankine Cycle (ORC) model

Rankine cycles are used to obtain electric power in a turbine from a heat source. In the case of ORCs, the objective is to convert the heat from a low-temperature heat source into useful electric power. In order to increase the efficiency and the net power output of the cycle, compared to steam Rankine cycles, organic compounds are used as working fluids as they show a better performance than water in these conditions of low temperature availability of the heat[19,20].

Among the possible configurations of ORCs, we distinguish between pure working fluid ORC (b), or just ORC, when the working fluids is a pure organic compound, and blend ORC (c) when the working fluid used is a mixture of two, or more, organic compounds. Additionally, depending on the condition of the fluid at the output of the evaporator, superheated cycles (b), if the output of the evaporator is a superheated vapour, and partially evaporated, if the output is in the vapour-liquid phase, can be implemented (Fig. 20).

An ORC operates following the next schema: a saturated liquid at pressure p_1 [1], is compressed in a pump to a pressure p_2 [2], then the fluid is heated until a saturated liquid at pressure p_2 is obtained [2'], the fluid is evaporated [3'], and superheated ΔT_{sh}, until T_3 [3]. The pressure drop in the condenser is neglected, leading to a constant pressure in the whole heat exchanger. The power is generated by expanding the working fluid from [3] to a lower pressure, p_4 [4] in the turbine. Finally, the vapour is cooled until the saturation temperature [4'] and condensed, reaching the initial point [1]. As well as in the heater, the cooler is supposed to operate at constant pressure, neglecting any pressure drops. The common cycle is represented in the *T-s* diagram for a pure component in Fig. 20 (b).

The heat source is considered to have a constant heat flow, $\dot{m}_h c_{ph}$, and is characterised by three temperatures, the inlet temperature, T_{hi}, the outlet temperature, T_{ho}, and the pinch temperature, T_{hp}, that corresponds to the point of the heat exchanger in which the temperature difference between the heat source and the working fluid is the lowest. This point occurs when the heat source is at T_{hp}, and the working fluid at [2']. The cooling source is also represented by a constant heat flow, $\dot{m}_c c_{pc}$, and three temperatures, the inlet temperature, T_{ci}, the outlet temperature, T_{co}, and the pinch point of the cooler, T_{cp}. In this case the pinch is the temperature difference between T_{cp} and the saturated vapour [4'].

Cycles for blends have the same points as the pure ORC, but the main difference is the fact that evaporation and condensation temperatures are not constant, as shown in Fig. 20. In these cycles, another variable appears, which is the composition of each compound in the working fluid. Nevertheless, both models follow the same equations, indeed, one can consider the pure ORC as a blend cycle with a fixed composition of unity. The use of blends as the working fluid can improve the performance of the ORC, by improving the power output and the thermal efficiency [22].

For the partially evaporated cycles for pure working fluids, the superheat temperature, ΔT_{sh}, is equal to 0. Thermodynamic properties, mainly specific entropy and enthalpy, of [3] are calculated as a weighted property function of the vapour fraction and the liquid and vapour saturated properties. Points [4] and [4s] can also be in the liquid-vapour phase, depending on the conditions of [3]. In that case, their thermodynamic properties are calculated in a similar way.

The compression step (1 → 2) is characterised by the isentropic efficiency of the pump, η_{pump}, that is considered to have a fix value. For the expansion step (3 → 4), in the same way, a fixed value for the isentropic efficiency, $\eta_{turbine}$, for the expander is assumed.
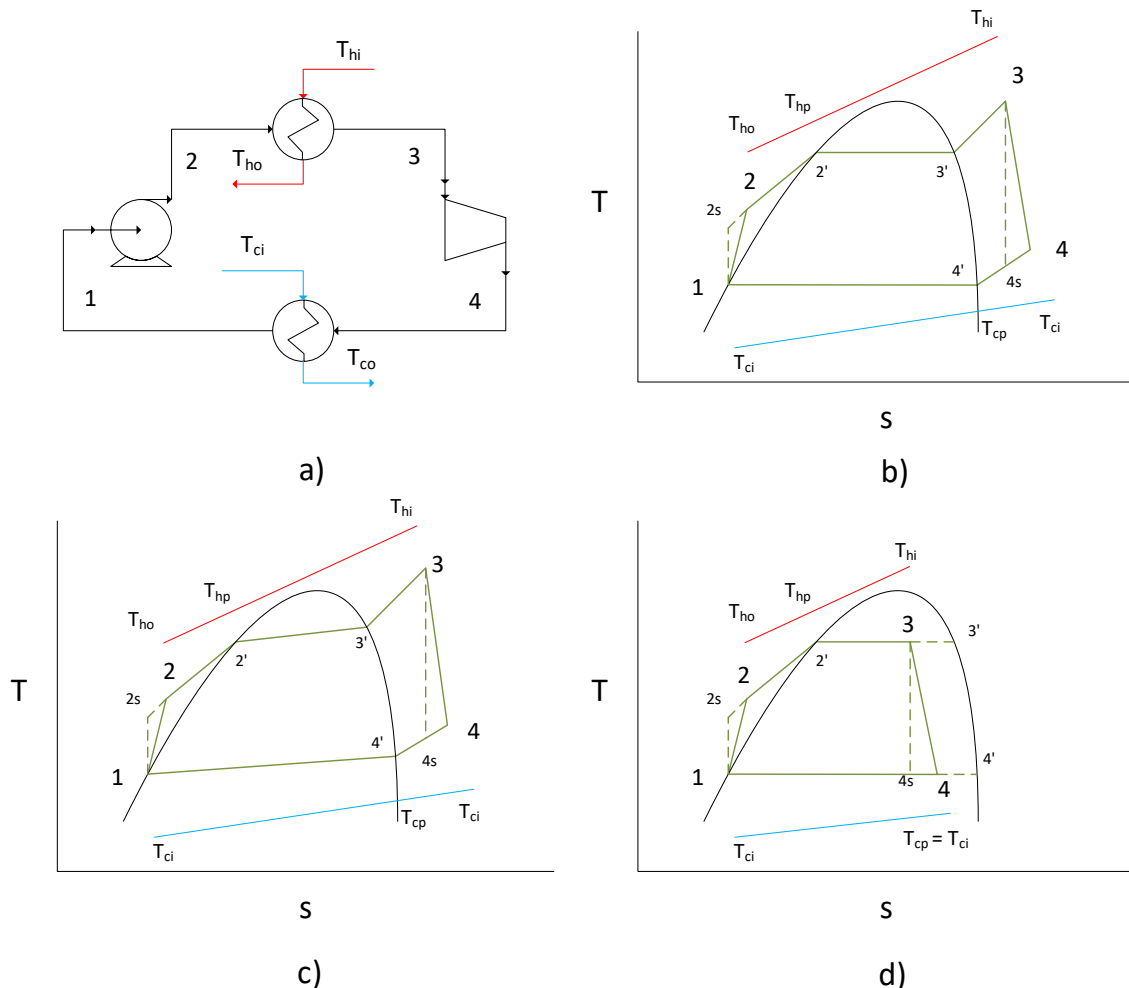

Fig. 20. a) ORC simplified flow diagram, with the main four stages. 1 → 2: compression. 2 → 3: evaporation. 3 → 4: expansion. 4 → 1: condensation. b) T-s diagram of an ORC with a pure working fluid, including the heat and cooling source. c) T-s diagram of an ORC with a blend as the working fluid. d) T-s diagram of a partially-evaporated ORC with a pure working fluid. Green: working fluid. Blue: cooling source. 1-4: ORC main states. s: isentropic process. ': at saturated conditions.

The model employed in the current work to obtain an optimal ORC, and then the optimal operation conditions and working fluid, is described below, including the equations. This model is a pure completely evaporated ORC (Fig. 20 b)). The variable z is a normalised variable used to characterised the outlet of the evaporator and it is characterised by

$$\begin{cases} x_{\mathrm{vap}} = z; & 0 \leq z < 1 \\ \Delta T_{\mathrm{sh}} = (z-1) \cdot (T_{hi} - T_{3'}); & 1 \leq z \leq 2 \end{cases} \qquad [64]$$

where x_{vap} is the vapour fraction and ΔT_{sh} the superheat temperature.

Compression stage 1 → 2

From saturated liquid at T_1 (1) the working fluid is compressed, with an isentropic efficiency [67], to a pressure p_2. The suffix 's' corresponds to the isentropic process, so the point 2s is the point at p_2 with the same entropy as the point 1. The suffix 'in' corresponds to the heat/power input to the system, whereas the suffix 'out' to the output of the system. This stage is characterised by the following equations.

$$T_1 = T^{sat}(p_1) \qquad [65]$$

$$s^{\mathrm{L}}(T_{2s}, p_2) = s^{\mathrm{L}}(T_1, p_1) \qquad [66]$$

$$\eta_{pump} = \frac{h^{\mathrm{L}}(T_{2s}, p_2) - h^{\mathrm{L}}(T_1, p_1)}{h^{\mathrm{L}}(T_2, p_2) - h^{\mathrm{L}}(T_1, p_1)} \qquad [67]$$

$$p_{2r} = \frac{p_2}{p_{cr}} \qquad [68]$$

$$w_{in} = h^{\mathrm{L}}(T_2, p_2) - h^{\mathrm{L}}(T_1, p_1) \qquad [69]$$

The reduced pressure in the evaporator, p_{2r}, is obtained with eq. [68], where p_{cr} represents the critical pressure of the working fluid calculated with the Joback-Reid[12] correlation [51]. The specific power of the pump, w_{in}, is calculated with eq. [69].

Evaporation stage 2 → 3

The working fluid is heated up until a saturated liquid is obtained (2′), then is evaporated (3′), and finally superheated to a temperature T_3. The following equations characterised the evaporation stage.

$$T_{2'} = T^{sat}(p_2) \qquad [70]$$

$$T_{3'} = T_{2'} \qquad [71]$$

$$T_3 = T_{3'} + \Delta T_{\mathrm{sh}} \qquad [72]$$

$$\Delta T_{\mathrm{sh}} = (z-1) \cdot (T_{hi} - T_{3'}) \qquad [73]$$

$$q_{\mathrm{in}} = h^{\mathrm{V}}(T_3, p_2) - h^{\mathrm{L}}(T_2, p_2) \qquad [74]$$

Variable z is a normalised variable to represent the extent to which the vapour is superheated [64]. The specific heat input, q_{in}, is obtained with eq. [74].

Expansion stage 3 → 4

From superheated vapour (3), the working fluid is expanded (4), obtaining a specific power, w_{out}. The expansion is characterised by an isentropic efficiency, η_{turbine} [76].

$$s^{\mathrm{V}}(T_{4s}, p_1) = s^{\mathrm{V}}(T_3, p_2) \qquad [75]$$

$$\eta_{\text{turbine}} = \frac{h^{\text{V}}(T_4, p_1) - h^{\text{V}}(T_3, p_2)}{h^{\text{V}}(T_{4s}, p_1) - h^{\text{V}}(T_3, p_2)} \qquad [76]$$

$$w_{out} = h^{\text{V}}(T_3, p_3) - h^{\text{V}}(T_4, p_4) \qquad [77]$$

Condensation stage 4 → 1

Finally, the fluid is cooled down to the saturated vapour (4') and condensed back to the initial point (1).

$$T_{4'} = T^{sat}(p_1) \qquad [78]$$

$$q_{out} = h^{\text{V}}(T_4, p_1) - h^{\text{L}}(T_1, p_1) \qquad [79]$$

An "if" condition is implemented to ensure both points, (4) and (4s), are out of the two-phase region and the working fluid is then superheated vapour.

Heat source

The heat source is defined by the heat flow, $\dot{m}_h \cdot c_{p,h}$, and three temperatures, the inlet temperature, T_{hi}, the outlet temperature, T_{ho} and the temperature at the pinch point, T_{hp}. All the heat released by the heat source is considered to be absorbed by the working fluid.

$$\dot{m}_{wf} = \frac{\dot{m}_h \cdot c_{p,h} \cdot (T_{hi} - T_{ho})}{q_{in}} \qquad [80]$$

$$\dot{m}_h \cdot c_{p,h} \cdot (T_{hi} - T_{hp}) = \dot{m}_{wf} \cdot \left(h^{\text{V}}(T_3, p_2) - h^{\text{L}}(T_{2'}, p_2) \right) \qquad [81]$$

$$PP_h = T_{hp} - T_{2'} \qquad [82]$$

The pinch point, [82], is the point at which the temperature difference between the heat source and the working fluid is the lower one. In the described model it occurs in the saturated liquid point (2') for the working fluid.

Cooling source

The cooling source is considered to be cooling water, with an inlet temperature of T_{ci}.

$$\dot{m}_{wf} \cdot q_{out} = \dot{m}_c \cdot c_{p,c} \cdot (T_{co} - T_{ci}) \qquad [83]$$

$$\dot{m}_h \cdot c_{p,h} \cdot (T_{cp} - T_{ci}) = \dot{m}_{wf} \cdot \left(h^{\text{V}}(T_{4'}, p_1) - h^{\text{L}}(T_1, p_1) \right) \qquad [84]$$

$$PP_c = T_{4'} - T_{cp} \qquad [85]$$

The cooling pinch point, [85], takes place at the saturated vapour point (4').

Finally, the performance of the cycle is measured with two variables, the thermal efficiency,

$$\eta_{th} = \frac{w_{out} - w_{in}}{q_{in}} \qquad [86]$$

and the net power output,

$$\dot{W} = \dot{m}_{wf} \cdot (w_{out} - w_{in}) \qquad [87]$$

Once the model equations and variables are collected, the resulting model is analysed to make it feasible. The structural analysis of the cycle involves solving the set of equations described above, incorporating the fixed values (see Table 18) that characterise the model. The total number of equations describing the model is 23, involving a total of 34 variables, some of which represent parameters that must be selected in order for the model to be completely specified.

The number of fixed variables to consider is seven. These values are summarised in the Table 18 and they were collected from literature to make the results comparable to other works of ORC optimisation[19,20,24].

Table 18. Constant values of the ORC model proposed.

η_{pump}	$\eta_{turbine}$	$\dot{m}_h \cdot c_{p,h}$ /kW $\cdot$ K^{-1}	$\dot{m}_c$ /kg $\cdot$ s^{-1}	$c_{p,c}$ /kJ $\cdot$ (Kkg)$^{-1}$	T_{ci} /K	T_{hi}/K
70%	80%	4.2	5	4.2	288	[423, 523, 623]

In addition to the constants of the model, some variables of the model are constrained. Table 19 collects the bounds, if considered, of the model variables.

Table 19. Bounds of the ORC model proposed

PP_c^L /K	p_1^L /bar	$\dot{m}_{wf}^L$ /kg $\cdot$ s^{-1}
5	0.25	0

The resulting parameter from the structural analysis are collected in Table 20. Besides these variables, the working fluid selection is considered. In the group contribution approach employed in the current work, a molecule is represented by the functional groups and their multiplicity.

Table 20. Parameters of the ORC model proposed

Parameters	Lower bound	Upper bond	Units
T_1	288	383	K
p_{2r}	0.001	0.85	-
z	1	2	-
PP_h	10	200	K

As a final step of the modelling of the ORC, the described model is implemented in gPROMS[29] and validated reproducing the same cycles simulated in some works of the bibliography[18–21], so the results are the same. By doing this last step, the model developed can be compared with the rest cycles of the bibliography, making the results comparable.

3.1.3. ORC optimisation

The performance of a Rankine cycle can be measured in several ways, nevertheless, two properties are widely used for this objective, the thermal efficiency, η_{th}, and the net power output, $\dot{W}_t$. First of all, the thermal efficiency, described in eq. [86], has been used as the reference of the cycle performance in several studies[18,54], and it has proved to be a good characteristic to optimise for low-temperature cycles, such as solar applications[55]. On the other hand, the net power output, described in eq. [87], is a crucial tool to measure the performance of the cycle and it has been used among several publications[18–20,56,57]. As shown in Fig. 30, the maximum thermal efficiency is obtained at the highest evaporator pressure, leading sometimes to negative power outputs, whereas the maximum power output is achieved at intermediate pressures, so both variables cannot be optimised with the same parameters. In this study, the net power is selected as the optimisation variable to be maximised, as it is considered to have a higher impact on the cycle performance.

As listed in the previous chapter (ref Chapter 2.3), the proposed ORC model has four degrees of freedom: the temperature in the condenser, T_1; the reduced pressure in the evaporator, p_{2r}; the

conditions of the output of the evaporator, z; and the working fluid, defined by the makeup of the molecule, in terms of the nature and number of its constituent groups. Therefore, the optimisation problem is a mixed integer non-linear programming (MINLP), as it concerns continuous variables, as well as integer variables for the working fluid description. This optimisation problem can be described with equations from [88] to [93].

$$\max_{x,y} \dot{W}_t(x,y) \tag{88}$$

Subject to:

$$h(x,y) = 0 \tag{89}$$

$$g(x,y) \leq 0 \tag{90}$$

$$Cn \leq d \tag{91}$$

$$x \in X \tag{92}$$

$$y \in Y \tag{93}$$

The net power output is set in equation [88] as the process variable to be maximised subject to the conditions set out in equations [89] to [93]. In equation [89], the set h represents the equality constraints of the problem, such as mass and energy balances or thermodynamic relations. On the other hand, the set of equations $g(x,y)$ [90] represents the inequality constraints of the problem that sets the bounds of the process variables. Equation [91] represents the bounds and restrictions for chemical feasibility of the working fluid considered. x indicates the set of continuous variables of the model [92], like the temperatures, pressures, etc., whereas y represents the discrete variables [93], in other words, the multiplicity of each contributing group of the working fluid.

To solve the resulting Mixed Integer Nonlinear Programming (MINLP) problem, an Outer-approximation (OA) framework is employed to solve the optimisation problem. This OA framework splits the optimisation problem in the primal problem and the master problem.

The primal problem, is the Nonlinear subproblem (NLP). It is the first step of each iteration, in which the nonlinear variables are set to constant values, turning the problem into an NLP problem.

The master problem, the Mixed Integer Problem (MILP), is defined by linearising the solution and the variables around the primal problem solution. The output of the master problem is employed in the next primal problem as the input variables.

The OA framework employed in the current work is a multiple start solver. Once the problem is initialised, the primal problem (NLP) is solved by fixing the integer variables, y, to constant values. If no feasible solution is found at this step, the primal problem is restarted. Otherwise, the variables and the objective function are linearised and the master problem (MILP) is attempted. This process is repeated until the termination criteria are reached. As a multiple start algorithm, the MINLP problem is solved until the maximum number of iterations is reached, being represented by the outer loop in Fig. 21. The termination criteria mentioned above refer to those operating conditions at which the objective function calculated, the net power output, is a local optima.
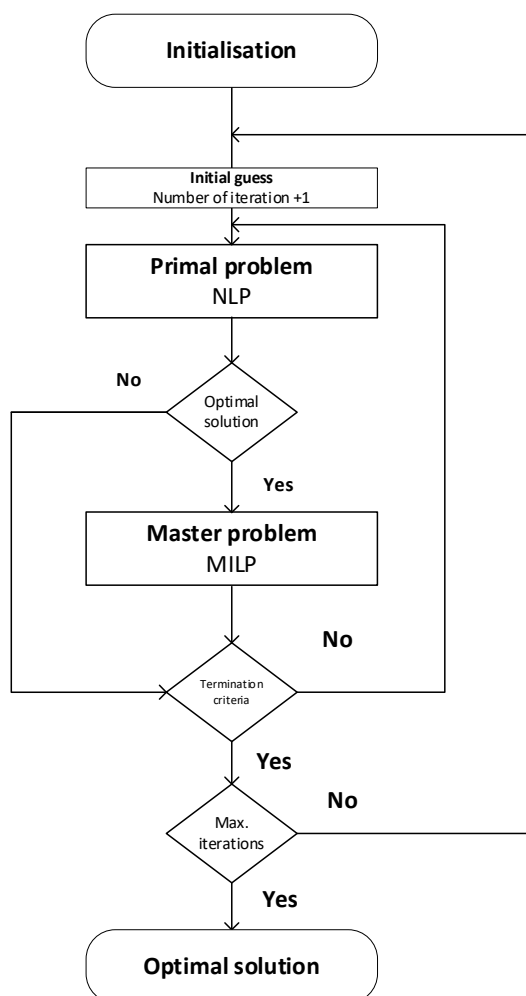
Fig. 21. Outer-approximation (OA) algorithm employed

Implementation

Both the ORC model and the optimisation problem are implemented in gPROMS[29]. Regarding the optimisation process described previously, the solution options configured in the software used are explained below.

The outer method selected to solve the MINLP is the NLPMSO solver of gPROMS, a multiple-start solver. Is an hybrid stochastic/deterministic approach for global optimisation by solving the optimisation problem in many initial guesses. The inner solver selected is an outer-approximation (OA) algorithm to solve the MINLP optimisation problems by splitting the problem in two subproblems, the primal problem (NLP) and the master problem (MILP); this solver is designated by the acronym OAERAP.

The NLP solver selected to solve the non-linear problem employs a sequential quadratic programming (SQP) method; this solver is designated as NLPSQP (NonLinear Programming Sequential Quadratic Programming).

The solver selected for the MILP subproblem, the master problem, uses a Branch-and-bound algorithm to cope with the integer variables of the system described; this method acronym is LPSOLVE, Linear Programming Solver.

3.2. Results and discussion

3.2.1. Thermophysical properties for ORC modelling

In this section, the transport properties of interest are analysed, comparing the experimental data from NIST/TRC Web Thermo Tables (WTT)[32] with the results from the correlations and methods explained in *3.1.1. Thermophysical properties for ORC modelling*. To analyse each property, the average absolute deviation is calculated for each property,

$$AAD\% = \frac{1}{N_R} \sum_{i=1}^{N_R} \frac{|R_i^{exp} - R_i^{calc}|}{R_i^{exp}} \cdot 100 \qquad [94]$$

where N_R is the number of data points of the property R, R_i^{exp} the experimental value of the property and R_i^{calc} the calculated one, at the ith conditions.

These properties are analysed for the compounds selected in Table 4, so trustable experimental data are available.

Normal boiling point

To estimate the normal boiling point, T_B, two methods are proposed, the Joback-Reid correlation[12] and the SAFT-γ Mie approach[3]. Both methods are analysed in order to select the more accurate one.

The results are plotted in Fig. 22, here the results for the same compounds calculated are plotted against the experimental data. The dashed lines represent a 10 K deviation between calculated and experimental data. Normal boiling point calculated with SAFT, the yellow diamonds, for all the compounds studied fall within the ±10 K deviation area. The Joback-Reid correlation, represented with the green circles, underestimates in some cases the normal boiling point, as the points are beneath the zero-deviation line.
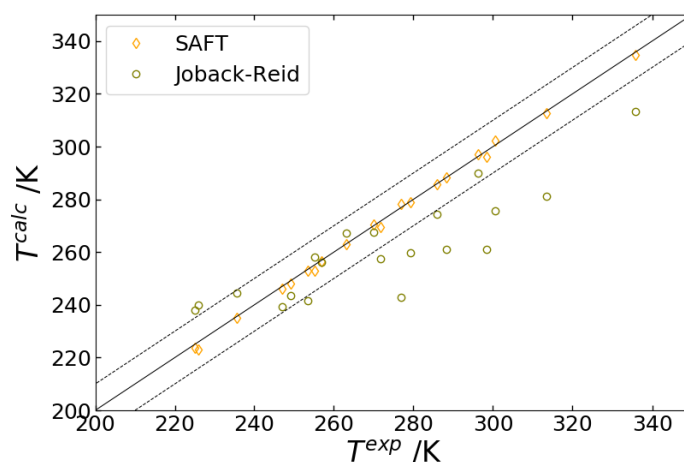

Fig. 22. Parity plot of calculated and experimental normal boiling point temperatures, T_B, highlighting T_B calculated using SAFT-γ Mie (orange open diamonds) and the Joback-Reid correlation (green open circles). Central line: parity line, calculated point equals experimental one. Dashed lines: ±10K deviation

The absolute deviation, AD, calculated for the SAFT-γ Mie is 0.97 K and 0.37% the average absolute deviation, AAD. For the Joback-Reid method, the AD is 14.37 K and the AAD obtained is 6.36%. Based on these results, the SAFT- γ Mie method is selected as the most suitable one to estimate the normal boiling point for the molecules studied in the current work.

Critical point

For the critical point temperature, pressure and volume, as well as in the boiling point, the SAFT method and the Joback-Reid correlation are proposed. Both methods are analysed for each property.

<u>Critical temperature, T_{cr}</u>

Critical temperatures calculated with both methods, T_{cr}^{calc}, are plotted against the experimental critical temperatures, T_{cr}^{exp} in Fig. 23. The dashed lines represent the ±10 K deviation area. The Joback-Reid method underpredicts the critical temperature in most of the compounds studied. For its part, results obtained with the SAFT method proposed tend to overpredict the critical temperature with a lower deviation than the other method.
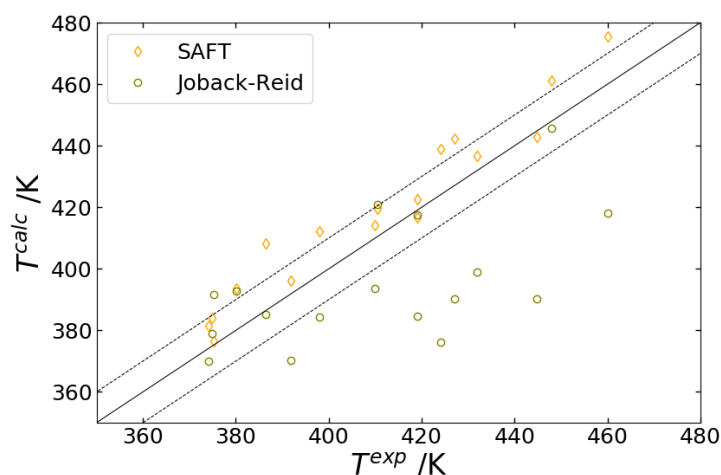

Fig. 23. Parity plot of calculated and experimental critical temperatures, T_{cr}, highlighting T_{cr} calculated using SAFT-γ Mie (orange open diamonds) and the Joback-Reid correlation (green open circles). Central line: parity line, calculated point equals experimental one. Dashed lines: ±10K deviation

The AD for the SAFT-γ Mie is 9.15 K and 2.30% the average absolute deviation, AAD. For the Joback-Reid method, the AD is 20.99K and the AAD obtained is 5.08%. In accordance with these results, the SAFT method is selected to estimate the critical temperature for the compounds.

<u>Critical pressure, p_{cr}</u>

The experimental and calculated critical pressures for the compounds of interest are plotted in Fig. 24, here the Joback-Reid correlation proves a better performance. The dashed lines define the ±0.5MPa deviation area.
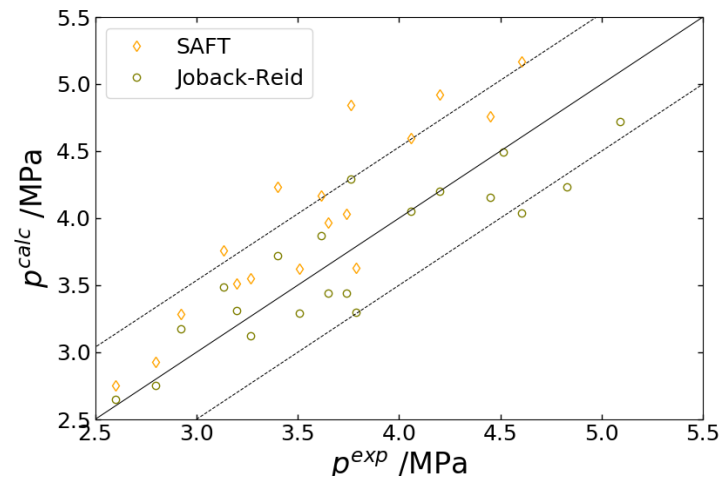
Fig. 24. Parity plot of calculated and experimental critical pressures, p_{cr}, highlighting p_{cr} calculated using SAFT-γ Mie (orange open diamonds) and the Joback-Reid correlation (green open circles). Central line: parity line, calculated point equals experimental one. Dashed lines: ±0.5MPa deviation.

With the SAFT-γ Mie method to calculate the critical point, the AD in the critical pressure obtained is 0.51MPa, with an AAD of 13.07%. With the Joback-Reid correlation, an AD of 0.24MPa is obtained, resulting in an AAD of 5.08%. Furthermore, this method does not overpredicts the critical pressure beyond the +0.5MPa deviation, whereas the SAFT method does, being useful to the further implementation of ORCs. Critical pressure of the working fluid is used to set the upper bound of the high pressure of the cycle. If the estimation overpredicts the critical pressure, cycle pressures over the desired bound are implemented in the ORC even though the reduce pressure will be inside the bounds.

Based on these results, the Joback-Reid method is found to perform a better estimation of the critical pressure, and is selected as the most suitable one for the current work.

Critical volume, V_{cr}

Just as for the other critical properties, the critical volume is analysed with the SAFT method proposed and with the Joback-Reid correlation. The results are plotted in Fig. 25, here the Joback-Reid correlation is found to have a better performance as all the points fall within the ±0.5dm^3·mol^{-1}. The critical volume obtained with the SAFT method have a big deviation from the experimental data, with a big dispersion.

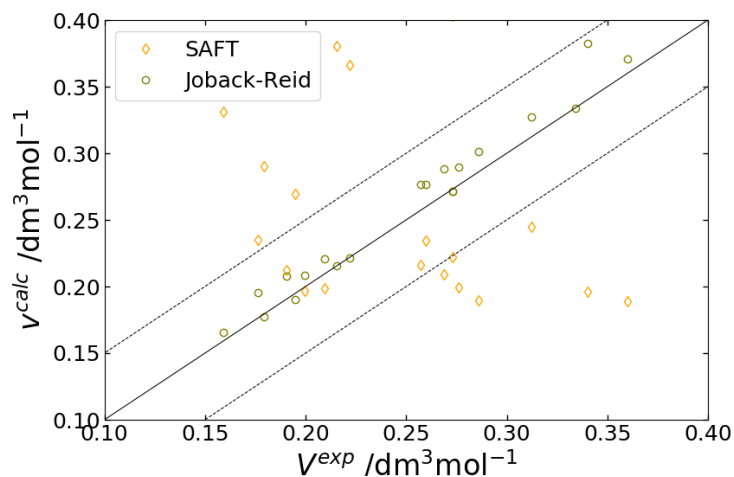*Fig. 25. Parity plot of calculated and experimental critical volumes, v_{cr}, highlighting v_{cr} calculated using SAFT-γ Mie (orange open diamonds) and the Joback-Reid correlation (green open circles). Central line: parity line, calculated point equals experimental one. Dashed lines: ±0.5dm³·mol⁻¹ deviation*

The AD obtained with the SAFT-γ Mie is 0.08, resulting in an AAD of 34.04%. For its part, the Joback-Reid correlation, the AD was 0.01 and an AAD of 4.29%. For this property, as for the critical pressure, the Joback-Reid correlation is selected, as the performance is better.

Surface tension

The surface tension, γ, calculated for some compounds is plotted in Fig. 27 (right) as a function of temperature. The continuous curves represent the correlation employed in the current work, and the points represent the experimental data from NIST/TRC[32]. The values of the calculated surface tension, γ^{calc}, are plotted against the experimental points, γ^{exp}, in Fig. 27 (left). Only the points that correspond to $T < 0.9 \cdot T_{cr}$ are collected in this plot, as the surface tension takes a value of zero at the critical point. The dashed lines represent the ±3mN·m⁻¹ deviation area, where all the points estimated are located. This method tends to overpredict the surface tension, as most of the points are above the equality line.

Fig. 26. Surface tension estimation (curves) and experimental data (points) for the selected compounds as a function of the temperature.
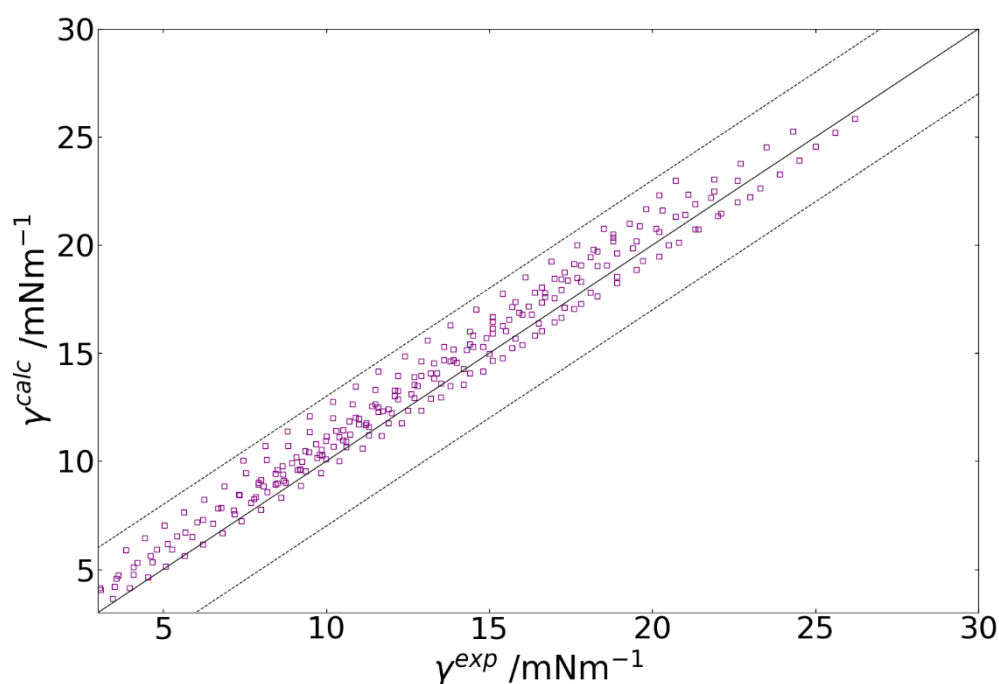
Fig. 27. Parity plot of calculated and experimental[32] surface tension, γ. Central line: equality line. Dashed lines: ± 3mN·m⁻¹ deviation.

This method results in an AD of 2.50 mN·m⁻¹ and an AAD of 9.30%. the deviation from the experimental points increases with the temperature. Nevertheless, the correlation used proves to be valid to estimate the surface tension of the fluorinated compounds studied, allowing further calculations for the ORCs.

Viscosity

For the dynamic viscosity, as for the thermal conductivity, two different correlations are used, one for each phase. Additionally, SAFT-γ Mie EoS is used to obtain the phase at the given conditions, and then the proper method used to estimate the viscosity. The results of the estimation are plotted in Fig. 28. The points represent the experimental data from NIST/TRC[32], and the curves the model proposed.

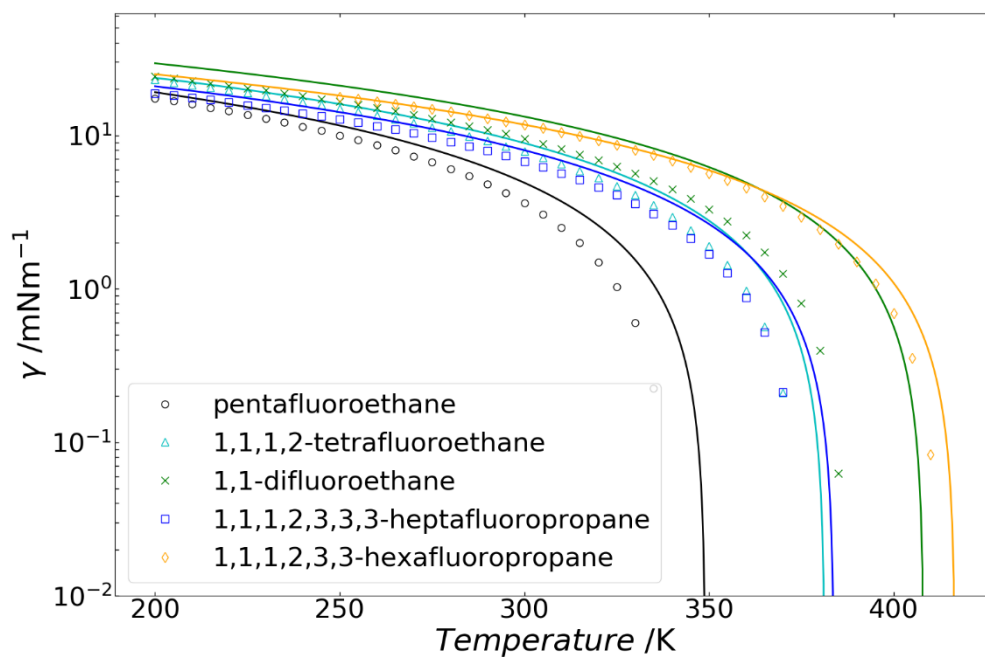*Fig. 28. Dynamic viscosity estimation (curves) and experimental data (points) for the selected compounds as a function of the temperature. y axis in logarithmic scale.*
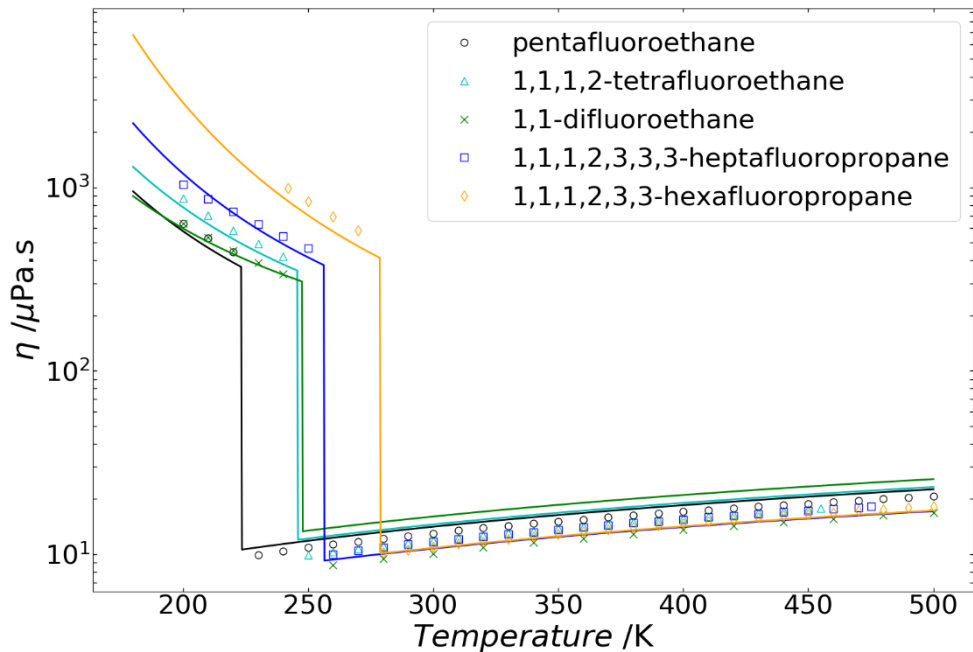
The AD from experimental data calculated, for the liquid viscosity, η_L, is 214.74 µPa·s, leading to an AAD of 15.16%. This error is taken into account for later calculations. The correlation used is designed to estimate the saturated liquid viscosity, so the pressure effect is analysed, at low pressures until 30 bar to ensure the correlation is available and accurate for the process of interest.

For the vapour viscosity, η_V, the AD estimated using the proposed method is 3.04 µPa·s, that means an AAD of 11.52%. The proposed method included a dipole moment correction factor, that is not suitable for a group contribution approach, so it was neglected for the current work, leading to bigger deviations. However, the deviation obtained is suitable to estimate the vapour viscosity for the compounds studied.

The viscosity of the working fluid can be estimated with the selected GC correlation. In spite of the deviations between the correlation and experimental data, the method proposed is useful to obtain the value, at different conditions and for a wide variety of working fluids, of both liquid and vapour viscosities. The importance of estimating the viscosity lies on the estimation of the ORC equipment size and the total cost[24].

Thermal conductivity

In Fig. 29 the thermal conductivity is estimated and plotted along with the experimental data gathered. As for the viscosity, a different correlation is used for each phase.
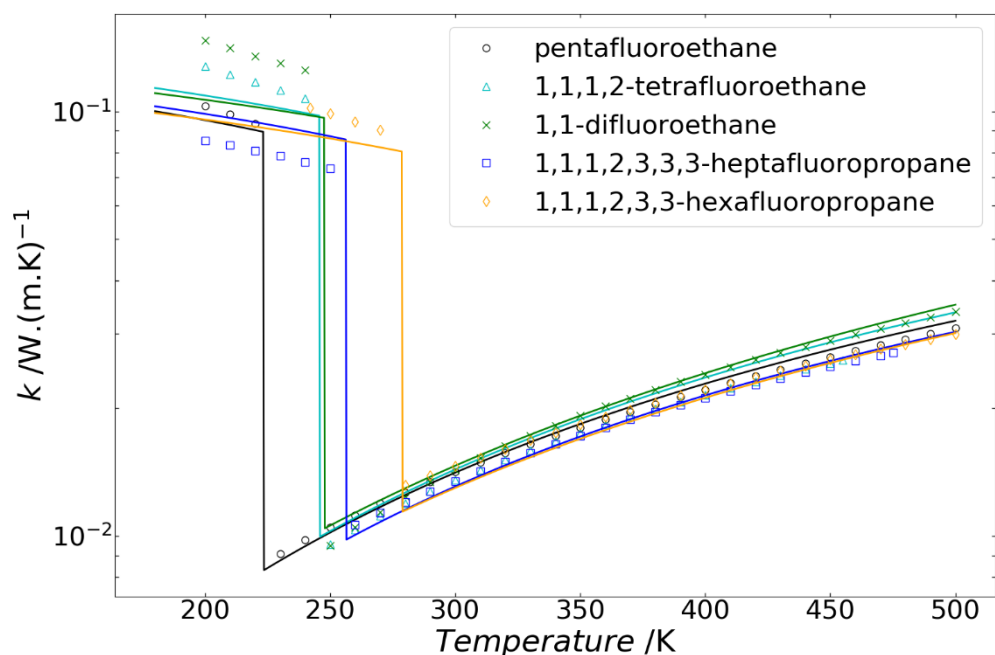
Fig. 29. Thermal conductivity estimation (curves) and experimental data (points) for the selected compounds as function of the temperature. y axis in logarithmic scale.

The liquid thermal conductivity, k_L, AD is 0.0166 W·(m·K)$^{-1}$, and the AAD 13.59%. It is evident from Fig. 29 that the correlation does not perform well in the liquid phase and is not completely trustable. This could be originated due to the suggestion made on the reference on using a correction factor not available for a group contribution approach. For this reason, the estimation has very different deviations for each molecule.

The proposed method to estimate the vapour phase thermal conductivity, k_V, obtained an AD of 0.0012 W·(m·K)$^{-1}$ resulting on an AAD of 4.77%. This method is suitable for the estimation of the vapour thermal conductivity for all the compounds studied.

The suitability of the correlations results for the compounds of interest, HFCs, is analysed in the plot and with the AADs, resulting in an adequate description of the thermal conductivity. The deviations from experimental data are acceptable for the purpose of the current work, as transport properties are not used within the ORC model nor the optimisation problem. Thermal conductivity, just as viscosity, is used in the sizing and cost estimation correlations.

Summary

The methods and correlations selected to estimate the main properties, described previously, are collected in Table 21, alongside with the absolute deviation, AD, and the average absolute deviation, AAD.

Table 21. Statistical analysis of the main fluid properties. AD: absolute deviation. AAD: average absolute deviation.

Property		AD	AAD %
Normal boiling point	T_B	0.97 K	0.37
Critical point	T_{cr}	9.15 K	2.30
	p_{cr}	0.24 MPa	5.08
	V_{cr}	0.01 dm^3·mol^{-1}	4.29
Surface tension	γ	2.50 mN·m^{-1}	9.03
Viscosity	η_L	214.74 µPa·s	15.16
	η_V	3.04 µPa·s	11.52
Thermal conductivity	k_L	0.0166 W·(m·K)$^{-1}$	13.59
	k_V	0.0012 W·(m·K)$^{-1}$	4.77

According to the results shown in the table, apart from the liquid saturation viscosity, the rest of properties have a deviation lower than 15%, making them suitable to estimate the properties of interest. Keeping in mind the fact that most of the correlations employed use some previously estimated properties, the results are encouraging. The objective of analysing these properties is to use them to estimate the cost of the ORC. However, a safety factor should be applied to collect the addition of this uncertainty originated from the use of group contribution methods and correlations.

3.2.2. ORC – CAMPD

ORC model validation

The ORC model is validated comparing the model developed in the current work with the results of other ORC from the references. Both papers used for the model validation, employ the same version of SAFT.

First of all, White et al. (2017)[20] analysed the effect of the reduced pressure in the net power output [87] and the thermal efficiency [86] of the cycle. The results of the cycle performed in the reference are represented with dashed lines in Fig. 30. The results with the cycle implemented in the current work for each compound are represented with the continuous lines.
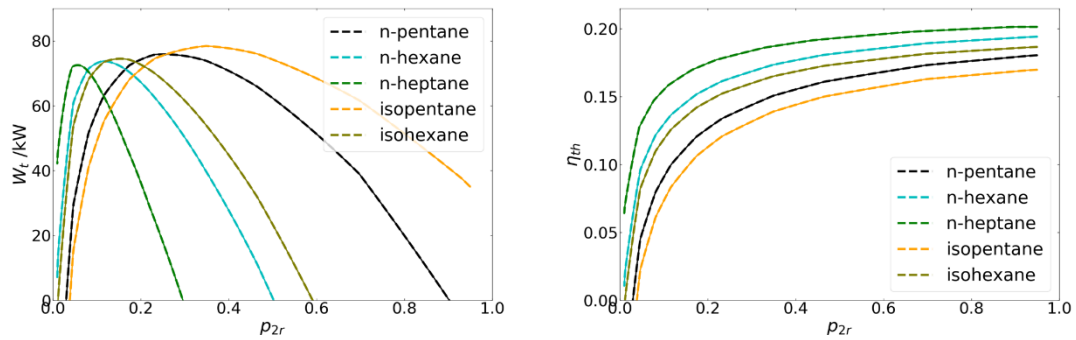
Fig. 30. Left: Net power output as a function of the reduce pressure in the evaporator, p_{2r}. Right: thermal efficiency as a function of the reduced pressure in the evaporator, p_{2r}. Lines: current work model. Dashed lines: reference model

As reflected in the figure, both models, the continuous and the dashed lines have the same trend and they are virtually indistinguishable from one another, concluding that the model implemented perform in a similar way, as the operating conditions and the thermodynamic approach employed are the same.

In the second paper, White et al. (2018)[19] considered either, partially and completely evaporated cycles. The variable z [64] represents the vapour fraction when it takes values from 0 to 1, and the extent of the superheat when takes values from 1 to 2. The power output is represented, for various values of the pressure in the evaporator, as a function of the variable z.
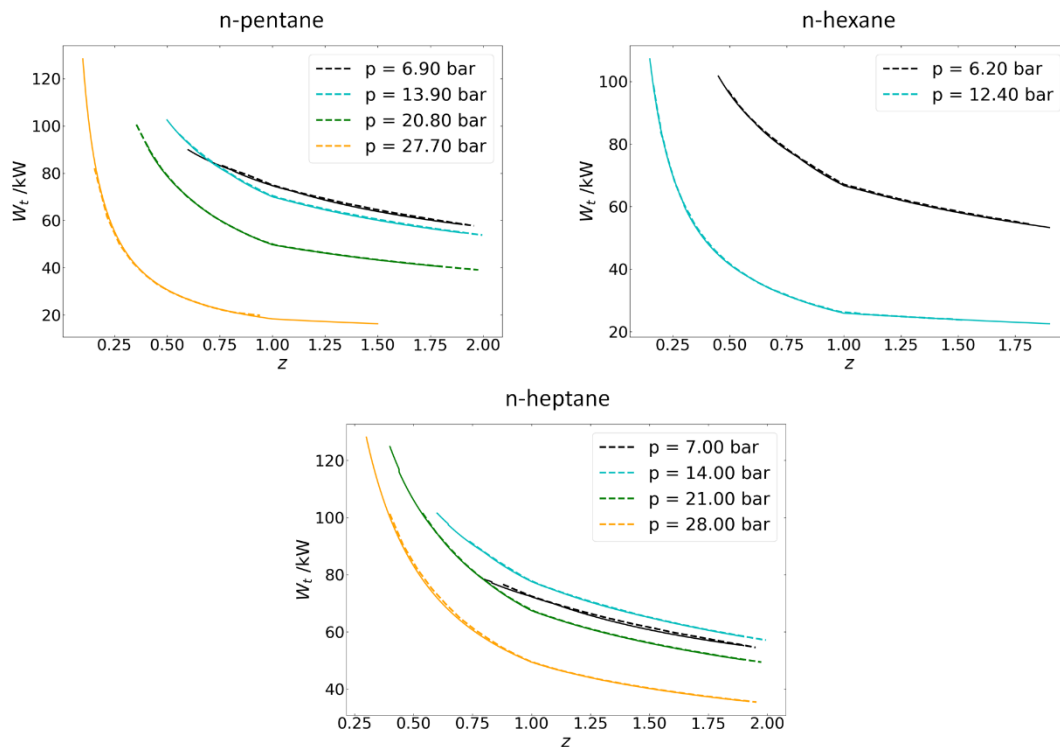
Fig. 31. Power output as a function of variable z for n-pentane (upper left), n-hexane (upper right) and isopentane (lower). Lines: current work model. Dashed lines: reference model

The dashed curves represent the cycle modelled in the reference, whereas the continues curves are from the current work. It can be concluded that the output of both models is essentially the same. There are no bigger deviations at either higher or lower values of the pressure in the evaporator.

Finally, it can be concluded that the ORC model implemented in the current work is able to represent other previously implemented cycle, obtaining the same values for the same operating conditions.

ORC optimiser validation

Once the ORC model implemented is validated, the NLP solver selection is validated, to ensure a correct behaviour of the solvers seleceted. To accomplish this step, results from two papers are selected.

Schilling et al. (2017)[23] presented the results of a CAMD optimisation of the ORC, optimising simultaneously the working fluid and the process variables. The equation of state employed in the reference is the PC-SAFT approach.

The outperforming working fluids obtained were selected to be optimised with the code used in the current work. In Table 22 the net power output obtained in the reference for each molecule is collected together with the optimised net power output obtained as a result of an NLP optimisation of the operation conditions.

Table 22. Net power output comparison between the Schilling et al. (2017) paper and the current work

Compound	Schilling et al.(2017)[23] W_{opt} /MW	Current work W_{opt} /MW	AAD
propane	1.59	1.66206	4.53%
propene	1.57	1.68429	7.28%
isobutane	1.56	1.59364	2.16%
isobutene	1.55	1.54633	0.24%
n-butane	1.55	1.56677	1.08%
1-butene	1.54	1.56001	1.30%
2-butene	1.53	1.53726	0.47%
neopentane	1.55	1.58206	2.07%
dimethyl ether	1.53	1.58448	3.56%
ethyl methyl ether	1.53	1.53824	0.54%

According to the results displayed in the table, the NLP solvers of both works, give a similar value of the optimal net power output for the given conditions. The differences between both works can be the fact that a different EoS is being used in, so the VLE and thermodynamic properties may differ, whereby small differences in AAD are inevitable.

In the previous work it was also reported the operation conditions of the optimal net power output of each working fluid. In Fig. 32 three of the operating conditions are compared for the optimal point. These conditions are the condenser pressure, p_1, (upper left figure), the evaporator pressure, p_2, (upper right) and the mass flow of working fluid, $\dot{m}_{wf}$ (lower).
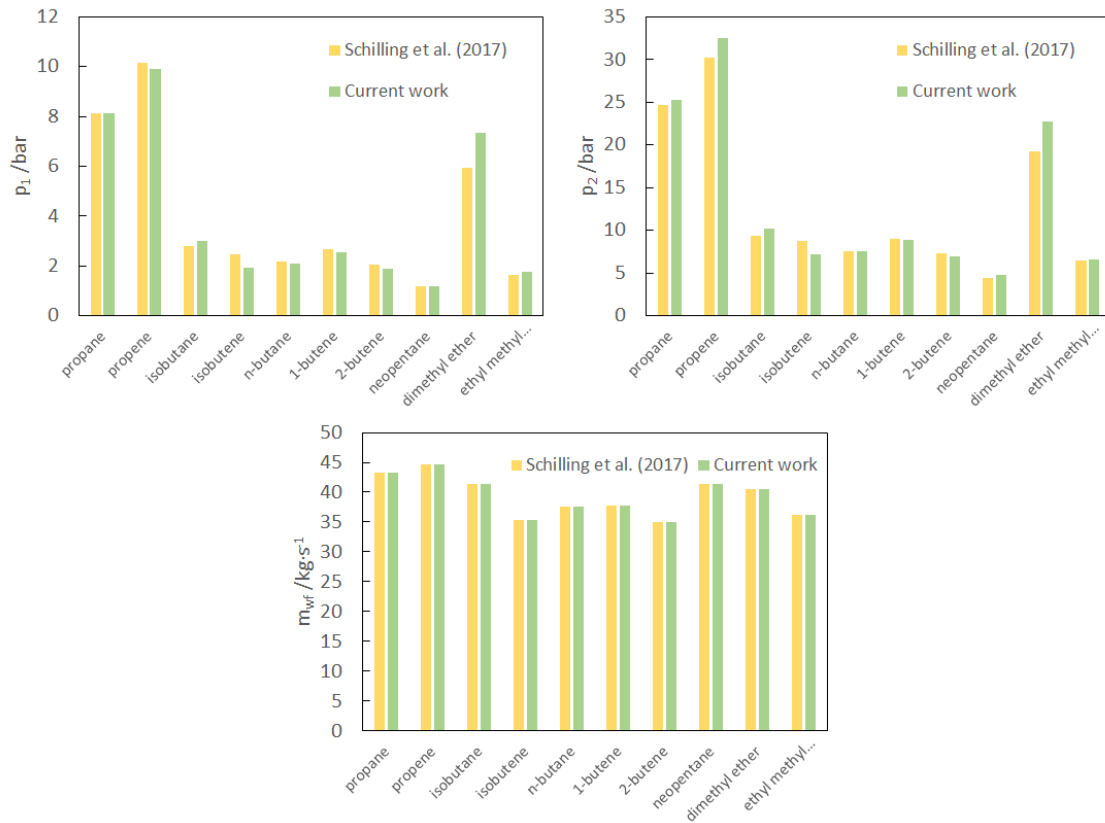
Fig. 32. Comparison of the optimised process variables for each compound between Schilling et al. (2017) reference and the current work. Upper left: condenser pressure. Upper right: evaporator pressure. Lower: working fluid mass flow.

As reflected in the three plots, not only the power output value is of the same order, but also both operating pressures, condenser and evaporator pressures, are of the same order. The mass flow rates of working fluid obtained for the optimal conditions take very similar values.

The second paper used is Bowskill et al. (2020)[18]. The operating conditions reflected in the papers were used to estimate the optimal net power output and the parameters to obtain that optimal point. The EoS used is SAFT-γ Mie, the same approach used in the current work. Both optimal points are collected, for two different conditions, in Table 23.

Table 23. Net power output comparison between the Bowskill et al. (2020) paper and the current work

Compound	Case I			Case II			
	Bowskill et al. (2020)[18] W_{opt}/MW	Current work W_{opt}/MW	AAD %	Bowskill et al. (2020)[18] W_{opt}/MW	Current work W_{opt}/MW	p_{2r}	AAD%
propane	1.662	1.66101	0.06	6.288	7.43469	0.8	18.24
propene	1.661	1.66272	0.10	5.779	6.76287	0.8	17.02
n-butane	1.567	1.56646	0.03	8.347	8.35181	0.8	0.06
1-butene	1.56	1.55979	0.01	8.185	8.50693	0.8	3.93
2-butene	1.537	1.53712	0.01	7.53	8.71895	0.8	15.79
butadiene	1.536	1.53584	0.01	6.496	8.83064	0.8	35.94
1-pentene	1.191	1.19092	0.01	5.828	5.82522	0.33	0.05
1,4-pentadiene	1.201	1.20039	0.05	5.771	5.76878	0.31	0.04
ethyl methyl ether	1.538	1.53807	0.00	7.45	7.23113	0.8	2.94
diethyl ether	1.164	1.1633	0.06	5.752	5.7497	0.32	0.04

For the case I, the results only differ a little, as reflected in the small AADs calculated. In the case of the case II, bigger deviations are obtained for some compounds. These deviations are found when the upper bound set for the reduce pressure in the evaporator is reached. The reduced pressure, $p_{2r} = p_2/p_{cr}$, depends on the critical pressure. In the current work, the critical pressure is estimated with the Joback-Reid correlation, as explained in the chapter *3.2.1. Thermophysical properties for ORC modelling*. In the reference, the critical pressure is estimated with the SAFT-γ Mie approach. A big difference when estimating the critical pressure has been reported previously in the current work. For the ORC model and optimisation, the important parameter is the pressure in the evaporator, the reduced pressure is used only to bound the pressures of the model, to operate in the subcritical region. Despite this deviation in some molecules in case II, the NLP solver used in the current work is valid to obtain the optimal operating conditions of ORCs.

At this point, the framework for the computer-aided molecular and process design has been analysed and implemented in gPROMS[29]. The optimal working fluid and operating conditions of ORCs determination by running the selected algorithm remains as future work.

4. Conclusions

Development of new functional groups

SAFT-γ Mie approach is used, in the current work, to estimate the pure and binary VLE, as some thermodynamic properties like enthalpies and entropies, heat capacities, coefficients of expansion and so on. These properties are useful for the thermodynamic modelling of cycles, in particular organic Rankine cycles (ORCs). SAFT-γ Mie belongs to the SAFT-type equations of state family and it is also a group-contribution method, making it suitable to evaluate the thermodynamic properties of the working fluids that can be formed from not only the available groups, but also the ones developed in the current work.

The first objective is the extend the range of application of SAFT-γ Mie approach. Previous works developed the framework to use this approach for alkanes, alkenes, branched alkanes, ethers, perfluoroalkanes and so on. Hydrofluorocarbons (HFCs) are alkanes in which some of the hydrogen atoms have been replaced by fluorine atoms. Then, the functional groups present in these compounds are alkyl, perfluoroalkyl and hydrofluoroallkyl groups. Hydrofluoroalkyl groups had not been developed within the SAFT-γ Mie in previous works, whereas the other groups are available.

HFCs are fluids with several applications, among which their use as working fluid in cycles is outlined. These compounds have replaced Chlorofluorocarbons (CFCs) in refrigeration cycles and they show a good performance as working fluid for power cycles, like ORCs. To enable the modelling of cycles that use HFCs as the working fluid, new groups are developed within the SAFT-γ Mie framework, allowing a complete thermodynamic description of this family of compounds.

To obtain the parameters needed to employ new groups within the SAFT-γ Mie approach, some selected properties, calculated with the model, are compared to experimental data, and then the parameters of the groups are optimised to obtain the best fitting. In this step, vapour pressure and saturated liquid density are commonly used to train the parameters. After the optimisation stage, the results obtained are validated by predicting other properties and comparing this prediction with experimental data available.

The parameters obtained in this work, corresponding to the hydrofluoroalkyl groups, are optimised to capture the VLE behaviour of some HFCs. This is done by fitting the calculated VLE, in particular vapour pressures and saturated liquid densities, to the experimental data from bibliography. The fitting is analysed, obtaining a good accordance between the VLE calculated with the model and the experimental VLE. To ensure an adequate functioning of the SAFT-γ Mie approach with the optimised parameters, some properties that are not used in the training stage are predicted and compared with the experimental data. These properties are the binary VLE and thermodynamic properties, such as specific enthalpies and entropies, isobaric heat capacities and other derivative thermodynamic properties. The model is validated for the thermodynamic properties, obtaining a good agreement with experimental data. In the case of binary VLE, the results are adequate for blends of similar HFCs, but when predicting the VLE of unsimilar HFCs it should be noted the failure of the proposed parameter to capture the VLE. To solve this issue, secondary-order group parameters should be used.

To conclude, the SAFT-γ Mie approach is a useful tool to model the thermodynamic behaviour of fluids. To use this approach to model the desired fluids, group parameters are needed. These parameters allow the use of the SAFT-γ Mie approach to reproduce the VLE behaviour of HFCs,

as well as predict fundamental properties, like calorific and thermodynamic ones. Regarding the binary VLE prediction, it should be noted that the developed parameters are able to predict the binary interaction in some cases, in those situations comprising unlike molecules, the proposed parameters are unable to predict the VLE. The parameters developed, along with the SAFT-γ Mie equation of state, are useful for thermodynamic modelling of cycles, like ORCs.

ORC analysis

Organic Rankine cycles (ORCs) are power cycles, as steam Rankine cycles or Kalina cycles, employed to obtain a power output using a heat source. In particular, ORCs employ organic compounds as working fluid to improve the thermodynamic performance of the cycle at certain conditions. They increase the power output, compared with steam Rankine cycles, when the heat source is available at a low temperature, making them more suitable to recover waste heat. ORCs are composed of four stages: compression, evaporation, expansion and condensation. The repetition of these four stages leads to obtaining a net power output. It can be distinguished between partially evaporated cycles, in which the output of the evaporator is a mixture of liquid and vapour, or completely evaporated cycles, where the output is a superheated vapour. In relation to the critical point, it can be distinguished between subcritical ORCs and supercritical ORCs, when the pressure in the evaporator takes values over the critical pressure. Regarding the working fluid, mixtures can be used, meaning a non-isothermal evaporation and condensation stages. In the current work the simplest cycle is considered, with a pure working fluid, subcritical and a completely evaporated cycle. However, the thermodynamic efficiency, together with the cost estimation, of other cycle configurations remains as a future objective.

The selected configuration of the ORC is modelled to analyse the performance of the HFCs as working fluid, as well as the operating conditions of the cycle. The SAFT-γ Mie approach is employed to model the thermodynamic properties of the working fluid of the cycle, through the four stages described above. The model is validated by comparing the output of the model with results from previous works, ensuring the same operating conditions lead to the same power output and process variables.

In addition to the thermodynamic modelling, other thermophysical properties are needed, to completely defined the ORC model. These properties are the critical point, the normal boiling point, the surface tension and transport properties. They are used to bound the cycle, ensuring and subcritical ORC and to implement the sizing and cost correlations.

The final objective would be to optimise the cycle, obtaining the optimal working fluid and the optimal conditions. To reach this objective, a computer-aided molecular and process design (CAMPD) framework is established, in which the net power output is set to be maximised modifying the operating conditions of the cycle and the working fluid employed. An outer-approximation (OA) algorithm is proposed to solve the resulting mixed integer nonlinear programming (MINLP) optimisation problem. The solution of this established optimisation problem remains as future work to be carried out. The simultaneous optimisation of the working fluid and cycle parameters is a crucial step to obtain an economically viable ORC.

To conclude, the model of ORC can be used to optimise the thermodynamic performance of the cycle, reaching the optimal conditions of the cycle. To provide a more detailed description of the cycle, including the equipment sizing and the cost estimation, transport properties models are analysed. These models are group contribution based, so the same working fluid description for the thermodynamic model (SAFT-γ Mie) and the transport properties model. The use of group contribution methods allows a higher number of molecules to be screened during the working

fluid selection. Finally, an optimisation of the ORC is proposed as future work. This optimisation tries to find the optimal working fluid for the ORC, formed with the functional groups developed in the first section and with previously estimated functional groups, and the optimal operating conditions for that working fluid, stablishing the computer-aided molecular and process design (CAMPD) framework.

Bibliography

1. Dufal S, Papaioannou V, Sadeqzadeh M, et al. Prediction of thermodynamic properties and phase behavior of fluids and mixtures with the SAFT-γ mie group-contribution equation of state. *J Chem Eng Data*. 2014;59(10):3272-3288. doi:10.1021/je500248h

2. Papaioannou V, Calado F, Lafitte T, et al. Application of the SAFT-γ Mie group contribution equation of state to fluids of relevance to the oil and gas industry. *Fluid Phase Equilib*. 2016;416:104-119. doi:10.1016/j.fluid.2015.12.041

3. Papaioannou V, Lafitte T, Avendaño C, et al. Group contribution methodology based on the statistical associating fluid theory for heteronuclear molecules formed from Mie segments theory for heteronuclear molecules formed from Mie segments. *Phys, J Chem*. 2014;054107. doi:10.1063/1.4851455

4. Soave G. Equilibrium constants from a modified Redlich-Kwong equation of state. *Chem Eng Sci*. 1972;27(6):1197-1203. doi:10.1016/0009-2509(72)80096-4

5. Peng DY, Robinson DB. A New Two-Constant Equation of State. *Ind Eng Chem Fundam*. 1976;15(1):59-64. doi:10.1021/i160057a011

6. Renon H, Prausnitz JM. Local compositions in thermodynamic excess functions for liquid mixtures. *AIChE J*. 1968;14(1):135-144. doi:10.1002/aic.690140124

7. Abrams DS, Prausnitz JM. Statistical thermodynamics of liquid mixtures: A new expression for the excess Gibbs energy of partly or completely miscible systems. *AIChE J*. 1975;21(1):116-128. doi:10.1002/aic.690210115

8. Fredenslund A, Jones RL, Prausnitz JM. Group-contribution estimation of activity coefficients in nonideal liquid mixtures. *AIChE J*. 1975;21(6):1086-1099. doi:10.1002/aic.690210607

9. Müller EA, Gubbins KE. Molecular-based equations of state for associating fluids: A review of SAFT and related approaches. *Ind Eng Chem Res*. 2001;40(10):2193-2211. doi:10.1021/ie000773w

10. Chapman WG, Gubbins KE, Jackson G, Radosz M. New reference equation of state for associating liquids. *Ind Eng Chem Res*. 1990;29(8):1709-1721. doi:10.1021/ie00104a021

11. Chapman WG, Gubbins KE, Jackson G, Radosz M. SAFT: Equation-of-state solution model for associating fluids. *Fluid Phase Equilib*. 1989;52(C):31-38. doi:10.1016/0378-3812(89)80308-5

12. Joback KG, Reid RC. Estimation of Pure-Component Properties from Group-Contributions. *Chem Eng Commun*. 1987;57(1-6):233-243. doi:10.1080/00986448708960487

13. Gross J, Sadowski G. Perturbed-chain SAFT: An equation of state based on a perturbation theory for chain molecules. *Ind Eng Chem Res*. 2001;40(4):1244-1260. doi:10.1021/ie0003887

14. Blas FJ, Vega LF. Thermodynamic behaviour of homonuclear and heteronuclear lennard-jones chains with association sites from simulation and theory. *Mol Phys*. 1997;92(1):135-150. doi:10.1080/002689797170707

15. Lafitte T, Apostolakou A, Avendaño C, et al. Accurate statistical associating fluid theory for chain molecules formed from Mie segments. *J Chem Phys*. 2013;139(15).

doi:10.1063/1.4819786

16. Burger J, Papaioannou V, Gopinath S, Jackson G, Galindo A, Adjiman CS. A Hierarchical Method to Integrated Solvent and Process Design of Physical CO2 Absorption Using the SAFT-γ Mie Approach. *AIChE J*. 2015;61(10):3249-3269. doi:10.1002/aic.14838

17. Bcs. Incorporated. Waste Heat Recovery: Technology Opportunities in the US Industry. *Waste Heat Recover Technol Oppor US Ind*. 2008:1-112. doi:10.1017/CBO9781107415324.004

18. Bowskill DH, Tropp UE, Gopinath S, Jackson G, Galindo A, Adjiman CS. Beyond a heuristic analysis: Integration of process and working-fluid design for organic Rankine cycles. *Mol Syst Des Eng*. 2020;5(2):493-510. doi:10.1039/c9me00089e

19. White MT, Oyewunmi OA, Chatzopoulou MA, Pantaleo AM, Haslam AJ, Markides CN. Computer-aided working-fluid design, thermodynamic optimisation and thermoeconomic assessment of ORC systems for waste-heat recovery. *Energy*. 2018;161:1181-1198. doi:10.1016/j.energy.2018.07.098

20. White MT, Oyewunmi OA, Haslam AJ, Markides CN. Industrial waste-heat recovery through integrated computer-aided working-fluid and ORC system optimisation using SAFT-Γ Mie. *Energy Convers Manag*. 2017;150:851-869. doi:10.1016/j.enconman.2017.03.048

21. Schilling J, Lampe M, Gross J, Bardow A. 1-stage CoMT-CAMD: An approach for integrated design of ORC process and working fluid using PC-SAFT. *Chem Eng Sci*. 2017;159:217-230. doi:10.1016/j.ces.2016.04.048

22. Oyewunmi OA, Taleb AI, Haslam AJ, Markides CN. On the use of SAFT-VR Mie for assessing large-glide fluorocarbon working-fluid mixtures in organic Rankine cycles. *Appl Energy*. 2016;163:263-282. doi:10.1016/j.apenergy.2015.10.040

23. Schilling J, Lampe M, Gross J, Bardow A. 1-stage CoMT-CAMD: An approach for integrated design of ORC process and working fluid using PC-SAFT. *Chem Eng Sci*. 2017;159:217-230. doi:10.1016/j.ces.2016.04.048

24. van Kleef LMT, Oyewunmi OA, Markides CN. Multi-objective thermo-economic optimization of organic Rankine cycle (ORC) power systems in waste-heat recovery applications using computer-aided molecular design techniques. *Appl Energy*. 2019;251(January):112513. doi:10.1016/j.apenergy.2019.01.071

25. Mie G. Zur kinetischen Theorie der einatomigen Körper. *Annanlen der Phys*. 1903;316:657-697.

26. Barker JA, Henderson D. What is "liquid" ? Understanding the states of matter. *Rev Mod Phys*. 1976;4. https://journals.aps.org/rmp/pdf/10.1103/RevModPhys.48.587.

27. Wertheim MS. Thermodynamic perturbation theory of polymerization. *J Chem Phys*. 1987;87(12):7323-7331. doi:10.1063/1.453326

28. Dufal S, Lafitte T, Haslam AJ, et al. The A in SAFT: Developing the contribution of association to the Helmholtz free energy within a Wertheim TPT1 treatment of generic Mie fluids. *Mol Phys*. 2015;113(9-10):948-984. doi:10.1080/00268976.2015.1029027

29. Process System Engineering. 2019. https://www.psenterprise.com/.

30. Hu P, Chen LX, Chen ZS. Vapor-liquid equilibria for the 1,1,1,2-tetrafluoroethane (HFC-134a)+1,1,1,2,3,3,3-heptafluoropropane (HFC-227ea) and 1,1,1-trifluoroethane (HFC-

143a)+2,3,3,3-tetrafluoroprop-1-ene (HFO-1234yf) systems. *Fluid Phase Equilib*. 2013;360:293-297. doi:10.1016/j.fluid.2013.09.056

31. Oguchi K, Murano A, Omata K, Yada N. Experimental Study of PVT Properties of HFC-125 (CHF2CF3). *Int J Thermophys*. 1996;17(1):55-64.

32. National Institute of Standards and Technology. NIST/TRC Web Thermo Tables (WTT). NIST Standard Reference Subscription Database 3 - Professional Edition. Version 2-2012-1-Pro. http://wtt-pro.nist.gov/.

33. Tuerk M, Zhai J, Nagel M, Bier K. *Measurement of the Vapor Pressure and the Critical State Variables of New Refrigerants*. 79th ed. Fortschr. Ber. VDI Z. Reihe 19; 1994.

34. Saleh B, Wendland M. Measurement of vapor pressures and saturated liquid densities of pure fluids with a new apparatus. *J Chem Eng Data*. 2005;50(2):429-437. doi:10.1021/je0497496

35. Holcomb CD, Van Poolen LJ. Coexisting densities and vapor pressures for R 143 from 314 to 401 K with new critical point property estimates. *Fluid Phase Equilib*. 1994;100(C):223-239. doi:10.1016/0378-3812(94)80011-1

36. Widiatmo J V., Sato H, Watanabe K. Saturated-Liquid Densities and Vapor Pressures of 1,1,1-Trifluoroethane, Difluoromethane, and Pentafluoroethane. *J Chem Eng Data*. 1994;39(2):304-308. doi:10.1021/je00014a025

37. Duan YY, Wang ZW, Meng L, Sun XY. Vapor pressure measurements of 1,1,1-trifluoroethane (HFC-143a) and 1,1,1,3,3,3-hexafluoropropane (HFC-236fa). *Fluid Phase Equilib*. 2004;225(1-2):101-106. doi:10.1016/j.fluid.2004.08.015

38. van der Gulik PS. Viscosity of saturated R152a measured with a vibrating wire viscometer. *Int J Thermophys*. 1995;16(4):867-876. doi:10.1007/BF02093469

39. Feng X, Xu X, Lin H, Duan Y. Vapor pressures of 1,1,1,2,3,3,3-heptafluoropropane, 1,1,1,3,3,3-hexafluoropropane and 1,1,1,3,3-pentafluoropropane. *Fluid Phase Equilib*. 2010;290(1-2):127-136. doi:10.1016/j.fluid.2009.08.023

40. Duan YY, Shi L, Zhu MS, Han LZ, Lei X. Surface tension of pentafluoroethane and 1,1,1,2,3,3,3-heptafluoropropane. *Fluid Phase Equilib*. 2000;172(2):237-244. doi:10.1016/S0378-3812(00)00375-7

41. Gruzdev VA, Khairulin RA, Komarov SG, Stankus S V. Thermodynamic properties of HFC-236ea. *Int J Thermophys*. 2008;29(2):546-556. doi:10.1007/s10765-007-0369-6

42. Laesecke A, Defibaugh DR. Viscosity of 1,1,1,2,3,3-hexafluoropropane and 1,1,1,3,3,3-hexafluoropropane at saturated-liquid conditions from 262 K to 353 K. *J Chem Eng Data*. 1996;41(1):59-62. doi:10.1021/je950206t

43. Beyerlein AL, Desmarteau DD, Naik KN, Xie Y. *Physical Properties of Fluorinated Propane and Butane Derivatives and the Vapor Pressure of R245ca - R338mccq Mixtures as R-11 Alternatives*. 1st ed. ASHRAE Trans.; 1996.

44. Laesecke A, Hafer RF. Viscosity of fluorinated propane isomers. 2. Measurements of three compounds and model comparisons. *J Chem Eng Data*. 1998;43(1):84-92. doi:10.1021/je970186q

45. Marrucho IM, Oliveira NS, Dohrn R. Vapor-phase thermal conductivity, vapor pressure, and liquid density of R365 mfc. *J Chem Eng Data*. 2002;47(3):554-558. doi:10.1021/je015534+

46. Grosse A V., Wackher RC, Linn CB. Physical properties of the alkyl fluorides and a comparison of the alkyl fluorides with the other alkyl halides and with the alkyls of the elements of period II. *J Phys Chem*. 1940;44(3):275-296. doi:10.1021/j150399a002

47. Walker PJ, Haslam AJ. A new predictive group-contribution idel-heat-capacity model, and its influence on calorific properties calculated using a free-energy equation of state.

48. Sastri SRS, Rao KK. A simple method to predict surface tension of organic liquids. *Chem Eng J Biochem Eng J*. 1995;59(2):181-186. doi:10.1016/0923-0467(94)02946-6

49. Sastri SRS, Rao KK. A new group contribution method for predicting viscosity of organic liquids. *Chem Eng J*. 1992;50(1):9-25. doi:10.1016/0300-9467(92)80002-R

50. Horng TC, Ajlan M, Lee LL, Starling KE, Ajlan M. Generalized Multiparameter Correlation for Nonpolar and Polar Fluid Transport Properties. *Ind Eng Chem Res*. 1988;27(4):671-679. doi:10.1021/ie00076a024

51. Sastri SRS, Rao KK. A new temperature-thermal conductivity relationship for predicting saturated liquid thermal conductivity. *Chem Eng J*. 1999;74(3):161-169. doi:10.1016/S1385-8947(99)00046-7

52. Chung TH, Lee LL, Starting KE. Applications of Kinetic Gas Theories and Multiparameter Correlation for Prediction of Dilute Gas Viscosity and Thermal Conductivity. *Ind Eng Chem Fundam*. 1984;23(1):8-13. doi:10.1021/i100013a002

53. Reichenberg D. New methods for the estimation of the viscosity coefficients of pure gases at moderate pressures (with particular reference to organic vapors). *AIChE J*. 1975;21(1):181-183. doi:10.1002/aic.690210130

54. Papadopoulos AI, Stijepovic M, Linke P. On the systematic design and selection of optimal working fluids for Organic Rankine Cycles. *Appl Therm Eng*. 2010;30(6-7):760-769. doi:10.1016/j.applthermaleng.2009.12.006

55. Tchanche BF, Papadakis G, Lambrinos G, Frangoudakis A. Fluid selection for a low-temperature solar organic Rankine cycle. *Appl Therm Eng*. 2009;29(11-12):2468-2476. doi:10.1016/j.applthermaleng.2008.12.025

56. Oyewunmi OA, Kirmse CJW, Haslam AJ, Müller EA, Markides CN. Working-fluid selection and performance investigation of a two-phase single-reciprocating-piston heat-conversion engine. *Appl Energy*. 2017;186:376-395. doi:10.1016/j.apenergy.2016.05.008

57. Lampe M, Groß J, Bardow A. Simultaneous process and working fluid optimisation for Organic Rankine Cycles (ORC) using PC-SAFT. *Comput Aided Chem Eng*. 2012;30(June):572-576. doi:10.1016/B978-0-444-59519-5.50115-5

Symbols and abbreviations

Roman symbols

C	Coefficient
c	Specific heat, J·kg^{-1}·mol^{-1}
f	Function
g	Radial Distribution function
h	Specific enthalpy, J·mol^{-1}
K	Bounding volume
k	Thermal conductivity, W·(m·K)$^{-1}$
k_B	Boltzmann constant, J·K^{-1}
$\dot{m}$	Mass flow, kg·s^{-1}
$\dot{m}'$	Molar flow, mol·s^{-1}
n	Composition
n	Concentration vector
p	Pressure, Pa
PP	Pinch point, K
r	Centre-centre distance
S	Shape factor
s	Specific entropy, J·mol^{-1}·K^{-1}
T	Temperature, K
w	Specific power, J·mol^{-1}
$\dot{W}$	Power, kW
x	Mole fraction
z	Evaporator output condition

Greek symbols

γ	Surface tension, mN·m^{-1}
Δ	Increment
ε	Dispersive energy, m^2·kg·s^{-2} (J)
η	Efficiency
λ	ranges of the potential
μ	Viscosity, uds
v	Times a group is present in a molecule
v^*	Number of segments of a functional group
σ	Segment diameter, Å
$\varnothing$	Interaction potential

Subscripts

1-4	ORC states
A	Helmholtz free energy contribution
B	Normal boiling point
Bubble	Bubble point
C	Compounds
c	Cooling sink
cr	Critical
Dew	Dew point
e	Expander/turbine
G	Groups
h	Heat source
i	Inlet
k, l	Generic functional group of the SAFT-γ Mie approach
L	Liquid phase
N	Number of molecules
o	Output
obj	Objective
p	At the pinch point
p	Constant pressure
p	Pump
s	Isentropic

sat	Saturation conditions	assoc	Association contribution
sh	Superheat	c	Cut-off
ST	Site types, related with the association interaction	calc	Calculated with the SAFT-γ Mie approach
t	Total	chain	Chain contribution
V	Vapour phase	exp	Experimental
vap	Vapour pressure	HB	Hydrogen bounding
wf	Working fluid	HS	Hard sphere
Ω	Set of SAFT-γ Mie parameters	ideal	Related with the ideal contribution
i, j	Generic molecule	L	Lower bound
		mono	Monomer contribution

Superscripts

'	At saturation conditions	U	Upper bound
a	Attractive		

r   repulsive

Abbreviations

AAD   Average Absolute Deviation, %

AD   Absolute Deviation

CAMPD Computer-Aided Molecular and Process Design

CR   Combining rule

EoS   Equation of State

GC   Group-contribution

MILP   Mixed Integer linear programming

MINLP Mixed Integer NonLinear programming

NLP   Nonlinear programming

RDF   Radial Distribution Fraction

SAFT   Statistical Association Fluid Theory

VLE   Vapour-Liquid Equilibrium